The American Association of Petroleum Geologists Bulletin
V. 73, No. 1 (January 1989), P. 88-116, 21 Figs., 2 Tables

# Quantitative Analysis of North Sea Subsidence[1]

JULIAN A. THORNE[2] and ANTHONY B. WATTS[3]

## ABSTRACT

**Stratigraphic and geophysical maps of the northern and southern North Sea basin are used to study mechanisms of intracratonic basin formation. These maps include (1) tectonic subsidence for ten stratigraphic units, (2) predicted and observed sediment overpressure, (3) geographic variation of compaction constants, (4) net basement fault extension, (5) free-air gravity, (6) flexural rigidity, (7) heat flow, and (8) predicted hydrocarbon maturation.**

**In northern areas of the North Sea, observed basement-fault extension, crustal thinning, present-day flexural rigidity, and tectonic subsidence are predicted reasonably well by a simple stretching model of basin formation with rifting phases during the Triassic and mid-Jurassic/Early Cretaceous. In southern areas of the North Sea, however, a similar analysis suggests that other non-extensional rift-related processes dominated basin evolution. The effects of anomalously active aesthenospheric convection, coupled with basalt-eclogite and deep-crustal dewatering reactions, are considered as possible additional mechanisms.**

**The troughlike form of Quaternary tectonic subsidence suggests a new phase of rifting may be starting in the North Sea. The importance of such thermal rejuvenation is borne out by the association of areas of differential subsidence with high heat flow and low flexural rigidity. One component of tectonic reactivation during this period may be due to thermally induced isostatic reequilibration of older tectonic loads.**

## INTRODUCTION

The North Sea is a Paleozoic to Holocene multistage rift basin situated within the northwestern European cratonic block. The large amount of exploratory drilling in the area has provided a relatively thorough structural and stratigraphic description of this important hydrocarbon province (e.g., Woodland, 1975; Illing and Hobson, 1981; Ziegler, 1982). A major controversy exists, however, concerning the role of various lithospheric and crustal processes in causing the subsidence of the area. One school of thought, mainly within academic circles, believes that subsidence of the North Sea is mainly in response to some form of crustal extension (e.g., Sclater and Christie, 1980; Dewey, 1982; Wood and Barton, 1983; Barton and Wood, 1984; Beach, 1986). The other school, however, argues that reflection seismic data acquired by the petroleum industry precludes large amounts of crustal extension across the North Sea (Smythe et al, 1980; Ziegler, 1983).

Published isopach and structure contour maps, stratigraphic cross sections, as well as gravity, refraction, reflection, and well data in the public domain, can be used to test the applicability of the crustal extension model to the North Sea. Tectonic subsidence, extension on basin faults, thermal gradients, hydrocarbon maturation, and changes in crustal structure and lithospheric flexural rigidity are predicted by simple theoretical models of crustal extension during and after each rifting event (McKenzie, 1978; Sclater and Christie, 1980; Watts et al, 1982). In this study, we compare these predictions to the observed geologic history of the North Sea.

## TECTONIC SUBSIDENCE

One problem in the development of geophysical models to describe the North Sea is that the preserved stratigraphic record only indirectly reflects the tectonic processes responsible for basin evolution. Geohistory analysis (Van Hinte, 1978) can correct for compaction and paleowater depth to reconstruct the burial history of the sediments. The technique of backstripping (Steckler and Watts, 1978; Guidish et al, 1985), additionally evaluates the effects of eustatic sea level and the subsidence due to sediment loading. Each of these factors adds a component of subsidence to the primary tectonic driving force of basin subsidence. If the response to sediment loading is assumed to be local Airy isostasy, the tectonic subsidence, $\Delta Y$, for any interval of basin subsidence can be written

$$\Delta Y = (\rho_m - \rho_g)/(\rho_m - \rho_w)\Delta R + \Delta W + \Delta WD + \rho_m/(\rho_m - \rho_w)\Delta SL, \quad (1)$$

where $\rho_m$, $\rho_g$, and $\rho_w$ are the densities of mantle, average rock matrix, and water; $\Delta R$ is the observed solid isopach thickness (interval thickness normalized to 0% porosity); and $\Delta W$, $\Delta WD$, and $\Delta SL$ are the interval differences in net thickness of water in the sediment column, water depth, and eustatic sea level, respectively.

An analysis of the subsidence recorded in a small group of North Sea wells made by Sclater and Christie (1980) and Wood (1982) illustrated the importance of



[1]Manuscript received, April 8, 1985; accepted, May 15, 1987.

[2]Lamont-Doherty Geological Observatory and Department of Geological Sciences of Columbia University, Palisades, New York 10964. Present address: ARCO Research and Technical Service Company, 2300 W. Plano Parkway, Plano, Texas 75075.

[3]Lamont-Doherty Geological Observatory and Department of Geological Sciences of Columbia University, Palisades, New York 10964.

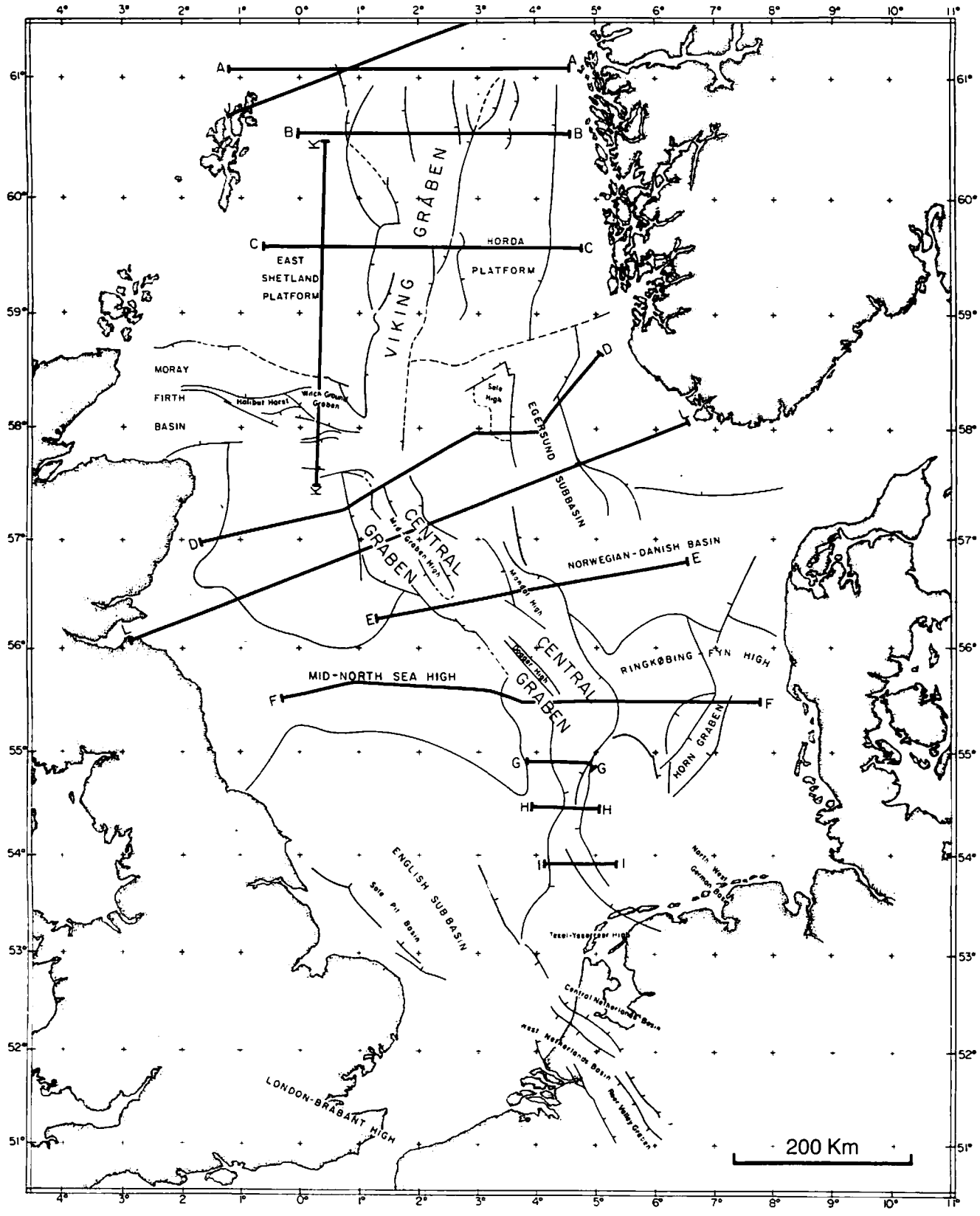


Figure 1—Location of structural features mentioned and cross sections used in this study. Names of features are from Day et al (1981) and Ziegler (1982). Cross sections and supplementary isopach maps from Caston, 1977; Day et al, 1981; Donatto, 1981; Finstad, 1975; Glennie et al, 1981; Heybroek, 1974, 1975; Pegrum et al, 1975; Pannekoek, 1954; and Ziegler, 1980.

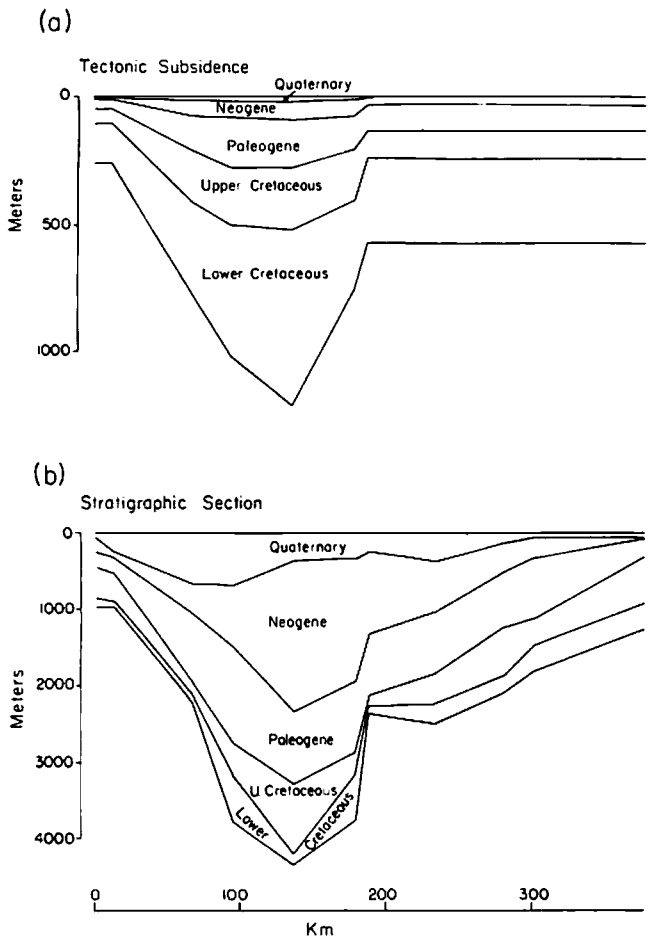


**Figure 2—(a) Approximations to equivalent tectonic subsidence of (b), as determined by Wood (1982) by best-fitting a theoretical subsidence curve through backstripped subsidence determined using technique of Sclater and Christie (1980). (b) Stratigraphic section through wells analyzed by Wood (1982). Note that relative thickness of deeply buried to shallow units is greatly increased in (a).**

backstripping. Figure 2a is a cross section (line LL in Figure 1) of the supra-Triassic sediments through the wells analyzed by Wood (1982). Figure 2b is a similar cross section where units of present-day thickness have been converted to units of tectonic subsidence using the porosity/depth relationship adopted by Sclater and Christie (1980). The relative importance of the Tertiary to the sub-Tertiary sediments is dramatically different after backstripping. In a reevaluation of North Sea porosity data, we will show, however, that the approximations made by Sclater and Christie (1980) may overestimate the effects of compaction in the North Sea.

### Errors in Estimating Tectonic Subsidence

Errors in estimating tectonic subsidence arise from uncertainties in any of the four terms on the right side of equation 1. The solid isopach thickness, $\Delta R$, is computed from stratigraphic age horizons and the average interval porosity, and $\Delta WD$ is computed from paleontological paleodepth indicators. Thus, $\Delta R$ and $\Delta WD$ are, in principle, directly observable from wireline logs, cuttings, core, or outcrop; but, in practice, $\Delta R$ and $\Delta WD$ are clearly subject to errors in interpretation. Eustatic sea level, $\Delta SL$, can be taken from one of the several published sea level curves in the literature (e.g., Watts and Steckler, 1979; Watts and Thorne, 1984; Haq et al, 1987). The uncertainty of this term can be important when studying the tectonic subsidence at a single well. The geographic pattern of tectonic subsidence for any interval, however, is not affected by the sea level correction term. $\Delta W$ is obtained by estimating the total amount of pore fluids contained in the sediment column as a function of time. This quantity cannot be directly measured but can be estimated by choosing a reasonable geologic model for compaction.

The size of $\Delta W$ is greatly affected by the overpressure gradient within the basin and the total thickness of the sediment column. The interval tectonic subsidence of a meter of slate, for example, can range between $\approx 0.3$ m ($\Delta W = 0$ m) and $\approx 3.3$ m ($\Delta W = 3$ m) depending on the average overpressure gradient and the depth to basement during deposition (see Appendix 1).

### Biostratigraphic and Downhole Geophysical Data

Biostratigraphic, lithological, and downhole geophysical information for over 200 wells in the North Sea area (Figure 3) have been digitally processed to prepare maps of tectonic subsidence. Isopach maps and cross sections published by various authors were used to supplement this information. Cross sections used in this study are shown in Figure 1. Equally spaced isopach values were computed on a Lambert's conic conformal projection at 27.8-km grid spacing. Our collected well data, where not overly influenced by salt diapirism, were weighted highly, compared to the supplementary sources within 55.6 km of each well.

### Compaction and Water-Depth Corrections

We made water-depth corrections to tectonic subsidence only for Cenozoic time-stratigraphic units. Corrections are based on the paleogeographic maps of Ziegler (1982), and calibrated by the minimum water-depth estimates in 19 wells from Wood (1982) and 16 wells from Berggren and Gradstein (1981).

Decompaction corrections made during backstripping consist of two parts: determination of porosities at the present time and extrapolation of these porosities into the past. Present-day porosities can be determined with a minimum of assumptions from downhole sonic or density logs. Extrapolation into the past when sediments were shallower is a more difficult problem.

Numerous review papers and texts have described the factors involved in loss of porosity in sediments undergoing burial (e.g., Rieke and Chilingarian, 1974; Magara, 1978). Loss of primary porosity is known to be a complicated process involving a combination of diagenetic

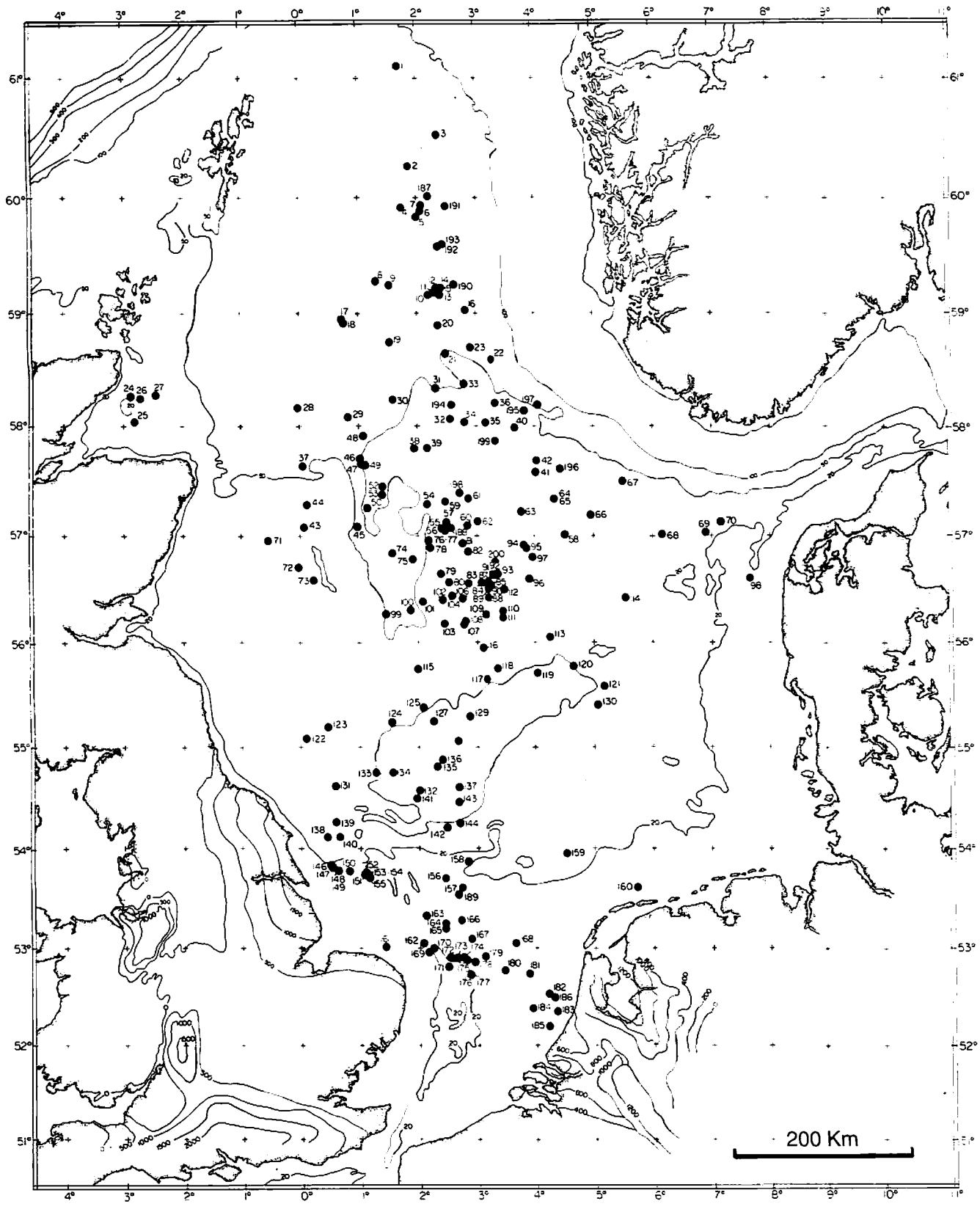


Figure 3—Location of 200 deep offshore wells used in this study. Offshore contours are of bathymetry in meters; onshore contours are of base Jurassic. Note that data density is greatest in axial regions of North Sea.

effects and mechanical compaction. The overall change in net porosity of a sedimentary basin, however, must simply be related to mechanical compaction because the pressure responsible for the expulsion of water from a sedimentary basin as a whole is derived only from sediment loading. A model based on mechanical compaction thus is appropriate in calculating tectonic subsidence, which requires a measure of $\Delta W$, the amount of pore fluids added, with additional deposition, to the entire sediment column.

### Mapping Present-Day Porosity

The simplest parameterization of mechanical compaction consists of empirical laws that relate average porosity to (maximum) burial depth and overall lithology (e.g., shale, sandstone, or chalk). Porosity in the North Sea cannot simply be predicted from these relationships because the same lithology at the same depth in different parts of the basin may have significantly different porosity (e.g., see Scholle, 1977). We instead have mapped porosity variations across the North Sea on the basis of downhole wireline logs. Porosity is derived mainly from sonic logs calibrated by density logs, cores (Hobbs and Long, 1977), and well-velocity surveys (United Kingdom Department of Energy open files).

Experimental work on the mechanical compaction of sediments (Poskitt, 1969; Skempton, 1970; Rieke and Chilingarian, 1974) as well as theoretical considerations (Biot, 1941; Lade, 1980) have shown that porosity, $\phi$, is simply related to effective pressure, p, by

$$\frac{\phi z}{1 - \phi z} = a(z) + b(z)\log_{10}\left[\frac{p(z)}{g}\right] = 6b(z) + b(z)\log_{10}\left[\frac{p(z)}{g}\right], \quad (2)$$

where a(z) and b(z) are compaction coefficients as a function of depth and g is the acceleration of gravity. The approximation $a(z) = 6\,b(z)$ is made based on data in Skempton (1970) for a wide range of North Sea sediments. The coefficient b(z) can be found as a continuous function of depth by back substituting measurements of downhole porosity and formation pressure. In practice, the function b(z) is noisy, expressing variations that may have little to do with mechanical compaction. We have suppressed this noise by first averaging over depth by time/stratigraphic unit, and second, modally averaging over the area between well-control points. Maps of the variation of compaction constant b have been prepared for ten stratigraphic units, two of which, the Eocene and Upper Cretaceous, are shown in Figure 4. These maps can be thought of as "compaction facies" maps showing the variation of lithology that leads to changes in compaction properties. Skempton (1970) also found a range of variation of compaction coefficient b from 0.25 to 0.75.

### Modeling Overpressure

A simple finite difference solution to the equations governing one-dimensional consolidation theory with overpressure is given in Appendix 1. Thus, the extent of overpressuring throughout basin history can be predicted from the previously described maps of sediment thickness and compaction constants, and the permeability constants given in Table 1. In Figure 5, a contour map of the predicted overpressure at the base of the Triassic at the present time is compared to individual downhole measurements. Appendix 1 lists predicted vs. observed downhole overpressure in six wells. The apparent success of the model indicates that, to a first order, burial rate probably is the key factor in the development of overpressure in the North Sea.

### Summary of Backstripping Procedure

Recent descriptions of the backstripping method can be found in Guidish et al (1985) or Bessis (1986). The procedure followed here involves several modifications as described in the previous sections. Briefly summarized, determining tectonic subsidence involves the following steps: (1) determine present-day stratigraphic thickness $S_i$ and paleowater depths, (2) estimate compaction coefficients $b_i$ (equation 2) from present-day porosity and pressure data, (3) estimate solid isopach thickness $\Delta R_i$ (equation 1) from interval thicknesses $\Delta S_i$ and compaction coefficients $b_i$, (4) model development of overpressuring within each interval from the loading history of the sediments and estimated interval permeabilities as a function of porosity (Appendix 1), (5) repeat steps two through four, changing estimates of interval compaction and permeability coefficients until a best fit is obtained to present-day observed pressure and porosity, (6) repeat step four one last time; with the application of each sediment load $\Delta R_i$, compute the change in effective pressure within each interval and, thus, the net change of water within the sediment column $\Delta W_i$, and (7) compute at each step the interval tectonic subsidence $\Delta Y_i$ from $\Delta R_i$, $\Delta W_i$, $\Delta WD_i$, and $\Delta SL_i$ (equation 1).

## TECTONIC SUBSIDENCE MAPS

Ten maps of tectonic subsidence are presented in Figure 6. These maps form the basis of a quantitative description of North Sea subsidence from the Triassic to the Holocene. The accuracy of these maps is hard to assess because the sources of error take many forms, ranging from uncertainties in the biostratigraphic information to uncertainties in the gridding, contouring, and interpolation procedures.

Two tests demonstrate that, on the whole, errors in backstripping are small. Figure 7a is an observed section across the Viking graben. The Tertiary, on the western flank of the basin, rests unconformably on metamorphic basement, and, in the center of the basin, the Tertiary is

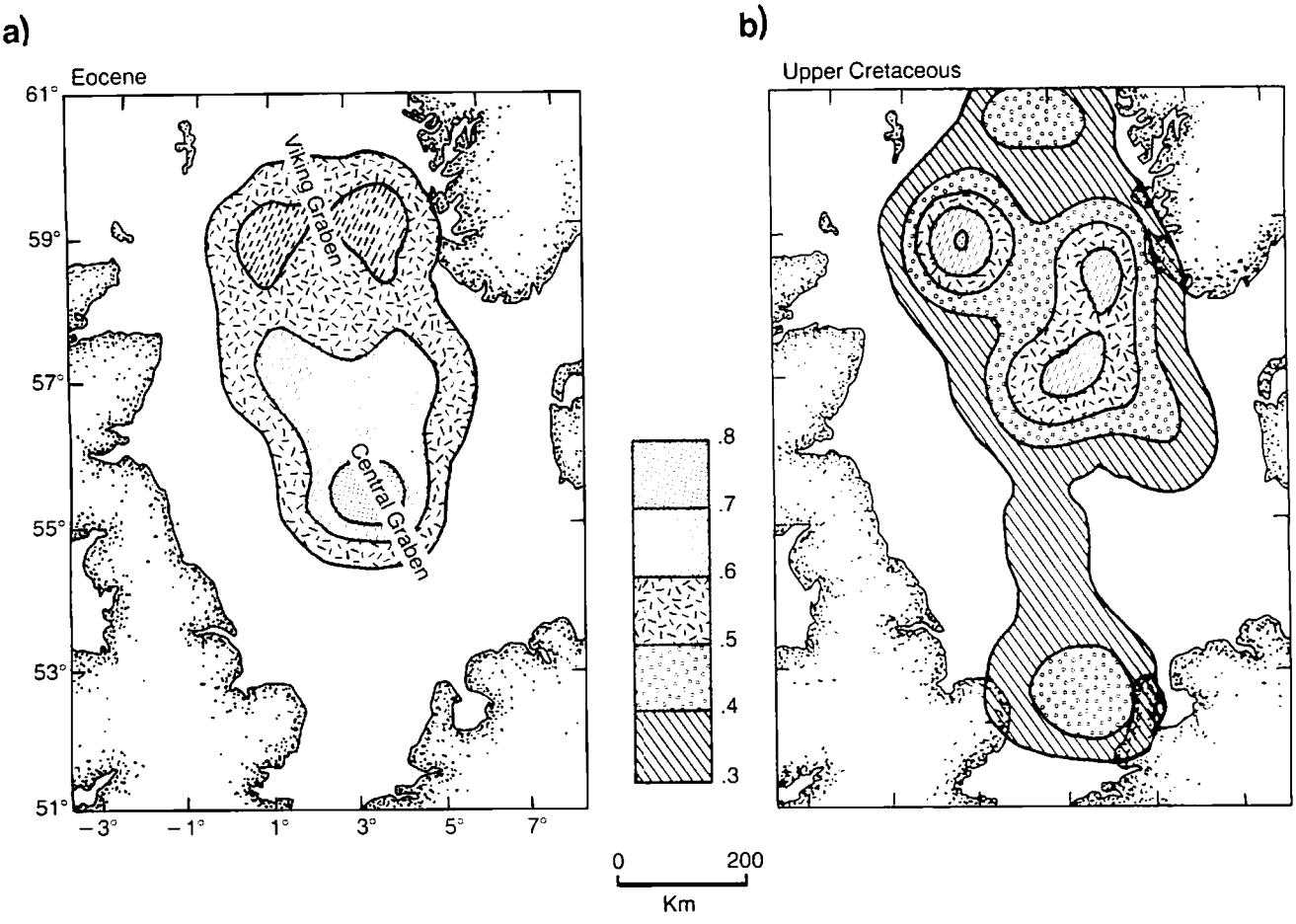


**Figure 4—Variation of compaction coefficient b(z) determined from porosity logs in wells shown in Figure 3. (a) Compaction coefficient for Eocene. (b) Compaction coefficient for Upper Cretaceous. Data have been smoothed and averaged as described in text. Variations in compactability represent changes in clay type in Eocene and chalk facies in Upper Cretaceous.**

underlain by a thick sedimentary section. Backstripped tectonic subsidence sections, using Sclater and Christie's method (Figure 7b) or the method presented here (Figure 7c), show contrasting results. Because of the strong effect of compaction corrections in Figure 7b, the tectonic subsidence of the Tertiary is higher on the west flank of the basin where it rests on basement than in the center. This tectonic "inversion" is probably an artifact of the backstripping method used. Following the procedure of backstripping outlined in the previous section, however, the maximum tectonic subsidence occurs, as expected, in the graben region (Figure 7c).

**Table 1. Permeability Constants**

| Time Interval | A* (from eq. 8A) | B* (from eq. 8A) |
|---|---|---|
| Quaternary | − 4.0 | 1 |
| Pliocene | − 4.0 | 1 |
| Miocene | −13.5 | 3 |
| Oligocene | −13.5 | 3 |
| Eocene | −13.5 | 3 |
| Paleocene | −13.5 | 3 |
| L. Cretaceous | −11.5 | 3 |
| E. Cretaceous | −11.5 | 3 |
| Jurassic | −13.5 | 3 |
| Triassic | −13.5 | 3 |
| Permian (Zechstein) | −12.5 | 0 |

*Determination of constants is from clay mineral analysis of Karlsson (1978).

Backstripping a sedimentary column is intended to recover the equivalent subsidence in water without the effects of sedimentary loading. The Quaternary subsidence presents an ideal case to test this equivalence and, therefore, the accuracy of our backstripping procedures. The tectonic subsidence map for the Quaternary (Figure 6a) shows a through-going trough running from north to south. Although this feature appears continuous, the tectonic subsidence in the north has been recovered mainly from an increase of water depth, whereas in the south, the reverse is true: sediment accumulation has recorded most of the tectonic subsidence. The magnitude of tectonic subsidence in the north is well known (the Pliocene was approximately at sea level and the present water depth can be measured directly). The magnitude of tectonic subsidence in the south, therefore, is constrained by the continuity of the feature observed in Figure 6a. The corrections made in determining tectonic subsidence, involving compaction of the entire sedimentary section, are consistent with this independent test.

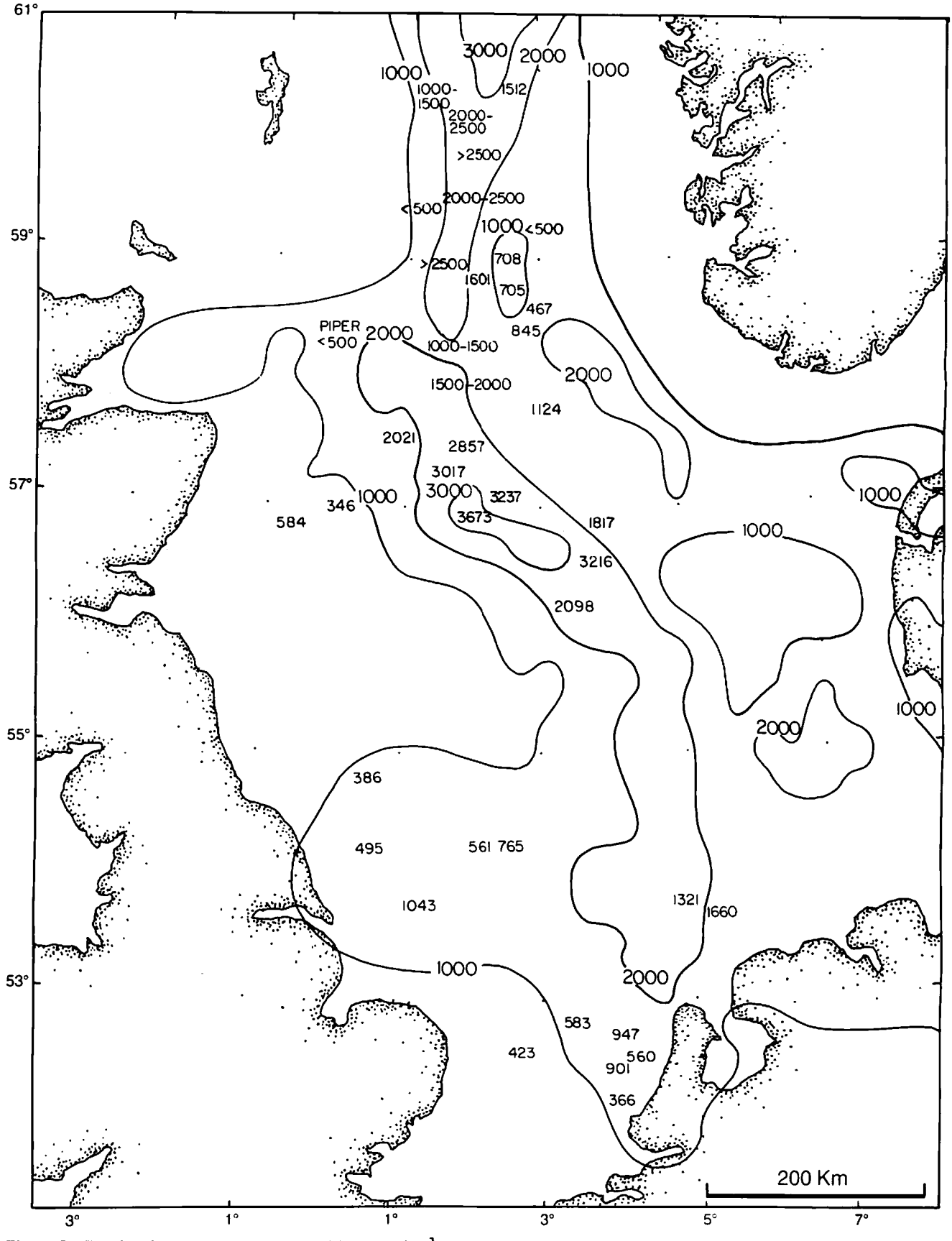


Figure 5—Predicted overpressure contoured in dynes/cm$^2$ at economic basement (base of exploratory wells in area). Numerical values, rounded to nearest 500, are from Chiarelli and Duffaud (1980). Other values are observed overpressures from borehole drill-stem tests.

## TESTING CRUSTAL EXTENSION MODEL

The evolution of a rift basin in which crustal extension plays a dominant role has been studied theoretically by a number of authors (e.g., Beaumont, 1978; McKenzie, 1978; Royden and Keen, 1980; Le Pichon and Sibuet, 1981; Watts et al, 1982). In the following section, we summarize briefly some of the concepts emerging from this work that can be used to quantitatively analyze the tectonic subsidence of the North Sea.

Generally, basin history can be divided into two styles of subsidence: (1) a rift phase of fault-controlled subsidence associated with active basin extension, and (2) a postrift phase of regional thermal subsidence due to cooling of the lithosphere. For the simple case of one short-lived rifting stage the approximate volume of tectonic subsidence in these two phases is given by equations 3-5 (modified from Le Pichon and Sibuet, 1981)

$$V_1(t = 0) \cong 3.61\,E, \tag{3}$$

$$V_2(t = \infty) \cong 4.22\,E, \tag{4}$$

$$V_T = V_1 + V_2(t = \infty) = 7.83\,E, \tag{5}$$

where E is the amount of crustal extension across the basin, t is the time since rifting, $V_1$ and $V_2$ are the volumes of tectonic subsidence per linear length of rift for the first and second phases respectively and the initial crustal thickness is 30 km. Equations 3 and 4 are not applicable to basins with a protracted rifting history in which extension may occur in several episodes. In this case , however, equation 5 holds for total extension and tectonic subsidence summed over all rifting stages.

The general trend of the subsidence is a rapid deepening during the rifting stage followed by a period of exponential decrease in the tectonic subsidence rate. A good test of the importance of thermal subsidence during the postrift phase is to match the one-dimensional solutions of McKenzie (1978) to observed subsidence by varying the parameter $\beta$: the ratio of the initial lithospheric thickness to the thickness after extension. If the width of the rift basin is narrow (< 50 km), however, significant cooling occurs by horizontal flow of heat. Loss of heat both horizontally and vertically accentuates the exponential character of basin subsidence (Steckler, 1981; Cochran, 1983).

An equally effective test for thermal subsidence is to measure quantitatively the tendency of subsidence to accelerate or decelerate with time. A particularly useful parameter is given by

$$C = \int_0^1 \mathring{a}(t')t'\,dt/[a(t_1) - a(t_2)] - 1, \tag{6}$$

where C is the concavity index of subsidence between $t_1$ and $t_2$, $t'$ is normalized time, $t' = t/(t_1 - t_2)$, and a(t) and $\mathring{a}(t)$ are the accumulation and accumulation-rate functions of tectonic subsidence. C has the advantage of being defined for any subsidence curve whether of thermal form or not. The index is positive for decelerating subsidence and negative for accelerating subsidence. The expected value of C for postrift thermal tectonic subsidence for any $\beta$ curve is given by (to within 5%)

$$C = 0.004t^{0.9}, \tag{7}$$

where t is greater than 15 m.y. and is time, in m.y., after rifting.

Extension models of basin formation also predict an elevation of the M-discontinuity (Moho) beneath graben areas of a rift basin. By simple isostatic arguments we can write

$$M = (\rho_c - \rho_w)/(\rho_m - \rho_c)V_T \cong 2.83V_T, \tag{8}$$

where $\rho_c$, $\rho_w$, $\rho_m$ are the crust, water, and mantle densities, respectively, M and $V_T$ are the volume of M-discontinuity topography and total tectonic subsidence per linear length of rift. From equations 5 and 8 we have

$$M = 22.17E. \tag{9}$$

Rifts with large amounts of crustal extension are also characterized by a diagnostic thermo-mechanical history. The role of lithospheric flexure, in particular, varies as a function of both time and position during the formation and decay of the thermal anomaly associated with basin rifting. To understand this, one must realize the lithosphere's ability to support vertically acting loads by bending stresses (its flexural rigidity) diminishes if heating of the lower crust or upper mantle allows high-temperature creep of quartz and olivine to occur (e.g., Kusznir and Karner, 1985). Rigidity also decreases where basin sediments are thick because elastic stresses relax quickly within sedimentary rocks (Warpinski, 1986). Laboratory experiments on creep and observations of flexure where the temperature structure is reasonably well known (Watts, 1978; Karner et al, 1983) have shown that flexural rigidity, D, is controlled by the depth below sedimentary basement of the 450°C isotherm, $Z_{450°C}$, such that

$$Z_{450°C}(\text{km}) = 2.24\text{E-}9D^{1/3} + B, \tag{10}$$

where D is in dyne/cm and B is the depth to basement. This relationship can be used to compare predicted depths to the 450°C isotherm and estimates of flexural rigidity D at various times during basin evolution. A good approximation of the depth to the 450°C isotherm in the axial regions of a graben where stretching factors are large ($\beta > 2$) is given by

$$Z_{450°C}(\text{km}) = 2.8\sqrt{t}, \tag{11}$$

where t is greater than 20 m.y. and is the time, in m.y., after cessation of rifting (Jarvis and McKenzie, 1980). During the postrift thermal subsidence stage, for example, the depth to the 450°C isotherm beneath the rift gradually increases as the lithosphere cools. Associated

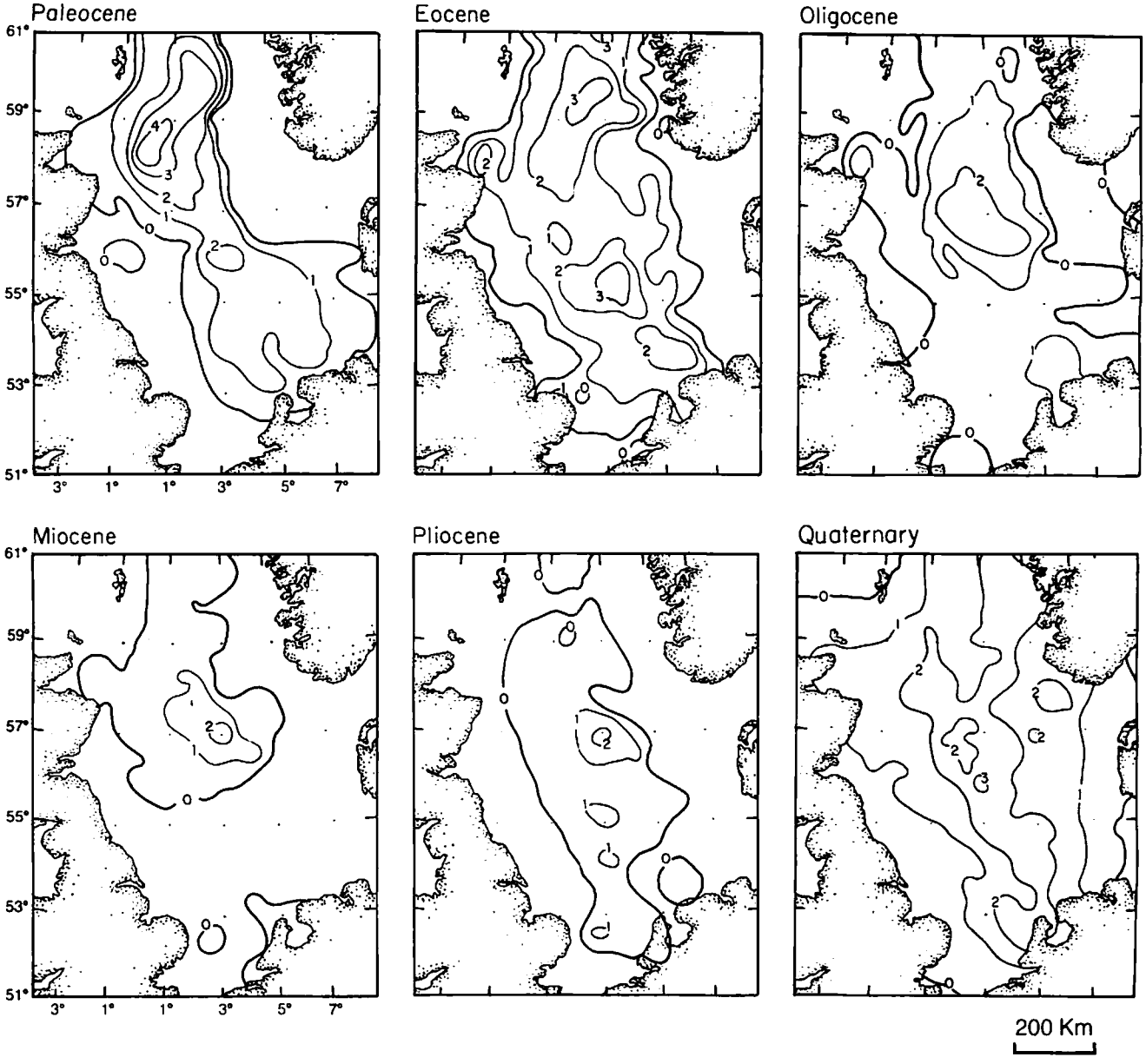


**Figure 6—Maps of tectonic subsidence for Cenozoic and Mesozoic units contoured at 100 m intervals. Location of 0 m contour is approximate. Water depth corrections have been made for Cenozoic units.**

with this deepening of the 450 °C isotherm is a progressive increase in the flexural rigidity of the lithosphere.

Estimates of D can be made from either of two methods: (1) free-air gravity and geoid anomalies (e.g., Watts et al, 1982; Barton and Wood, 1984) or (2) basin-load shape analysis (Haxby et al, 1976; Nunn, 1981; Ahern and Mrkvicka, 1984; Garner and Turcotte, 1984; Thorne, 1985).

In method one, a flexural rigidity is found such that predicted gravity anomalies arising from a flexural compensation model for basin sediments best fit the observed gravity variations across the basin. The inferred rigidity from this method reflects the average degree of isostatic compensation for sediment loads. As such, no information is obtained as to the time history of basin rigidity.

However, load-shape analysis, method two, can obtain rigidity estimates for different time/stratigraphic intervals. Rigidity is inferred from observed basin stratigraphy by a variety of methods. A brief description of three methods of load-shape analysis is given in Appendix 3.

In the next section, we analyze North Sea basin evolution using equations 3-11 to evaluate the applicability of simple extension models in this area. The Central and Viking grabens are discussed separately to underscore the differences between these two areas.

## CENTRAL GRABEN EVOLUTION

### Rift Stages

The first step in quantitative subsidence analysis is to divide basin evolution into periods characterized by

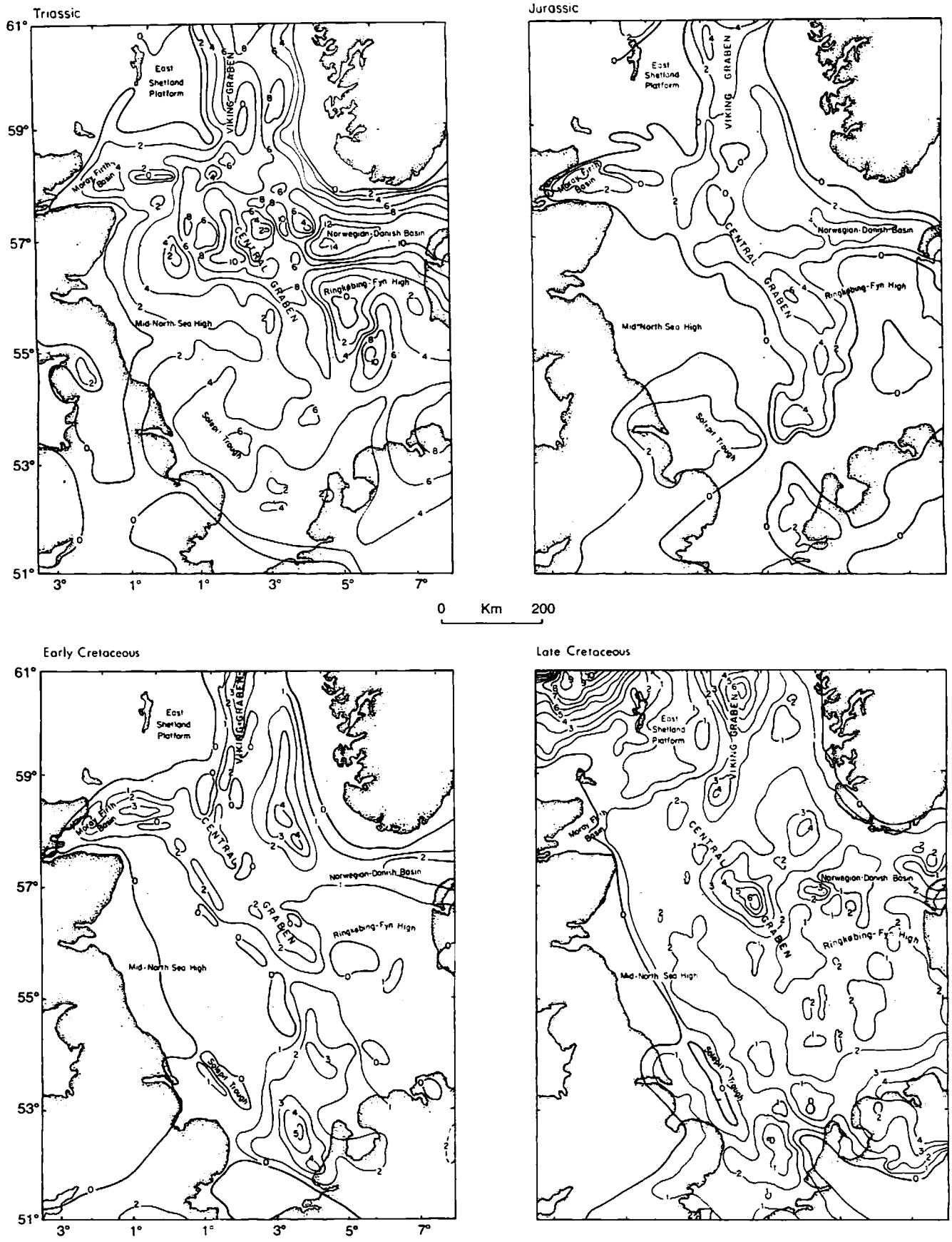


Figure 6 Continued.

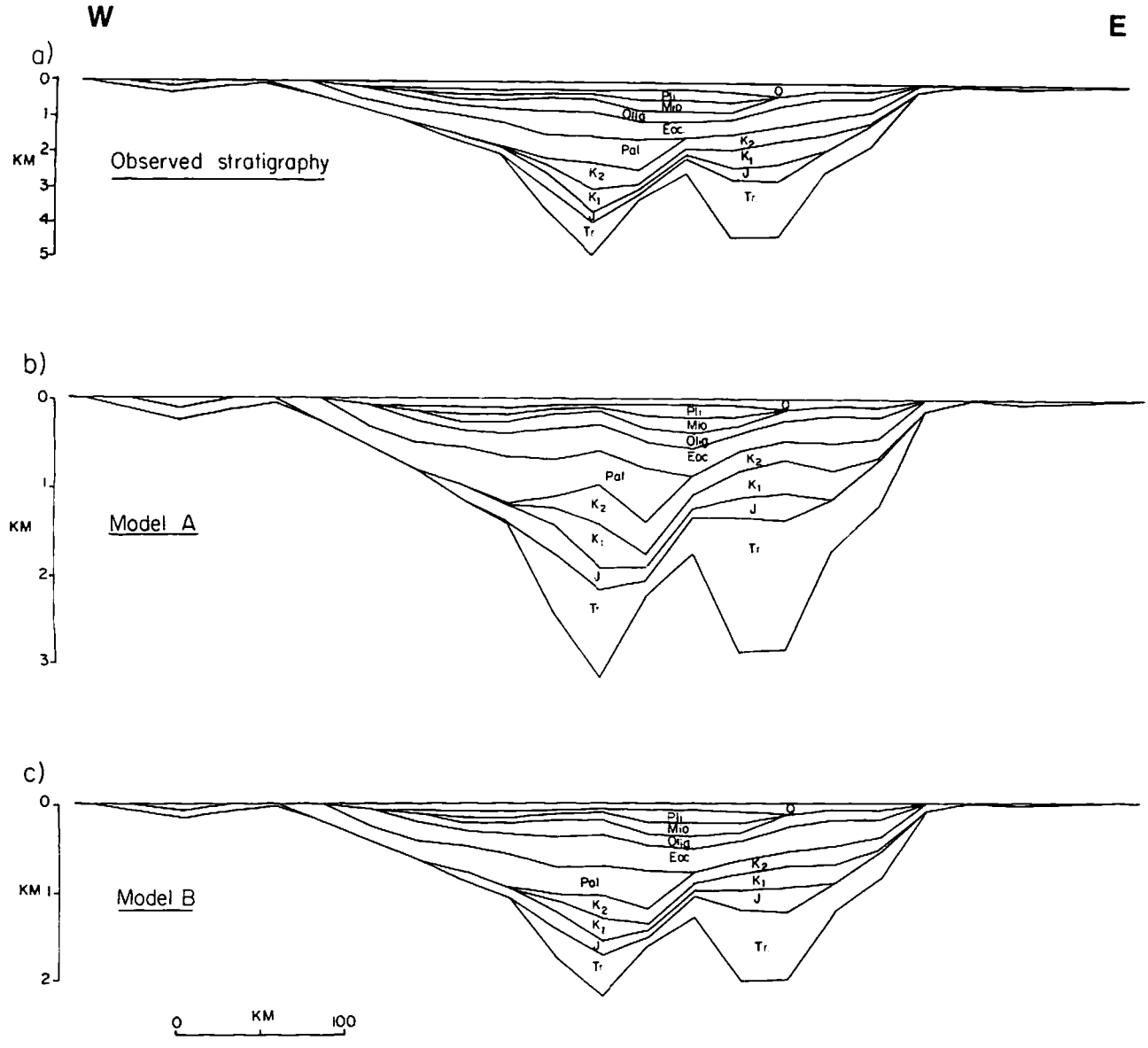


**Figure 7—(a) Cross section through Viking graben (at 59 °N latitude) extrapolated from equally spaced biostratigraphic information described in text. (b) Observed stratigraphy backstripped using method of Sclater and Christie (1980). (c) Observed stratigraphy backstripped by method presented in this paper. Note anomalous inversion structures in (b) introduced as artifact of backstripping.**

fault-controlled subsidence and periods characterized by regional subsidence. The timing of major periods of fault movement in the Central graben has been established by many writers using seismic reflection profiles across the basin (e.g., Maher, 1981; Hamar, 1983; Michelson and Anderson, 1983; Skjerven et al, 1983; Glennie, 1984; Gowers and Saeboe, 1985). Figure 8 schematically illustrates the results of these studies. Two phases of extensional faulting are distinguished. The first, occurring during the Late Permian to Early Triassic, appears on the cross section to be of greater importance than a second extensional stage from the mid-Jurassic to earliest Cretaceous. To our knowledge, no study has been done to quantitatively compare the amount and timing of fault extension on a regional basis.

The tectonic subsidence map of the Quaternary (Figure 6a) shows a broad trough-shaped region of subsidence greater than 100 m/m.y. This north-northwest-trending feature appears to reactivate the Central graben and Central Netherlands basin (see Figure 1). Other reactivated features include renewed subsidence in the Norwegian-Danish Trough and uplift of the Sole Pit basin.

### Regional Subsidence

The Upper Cretaceous and Tertiary of the Central graben area, in contrast, form a broad regional sag roughly centered over the underlying graben system. The change

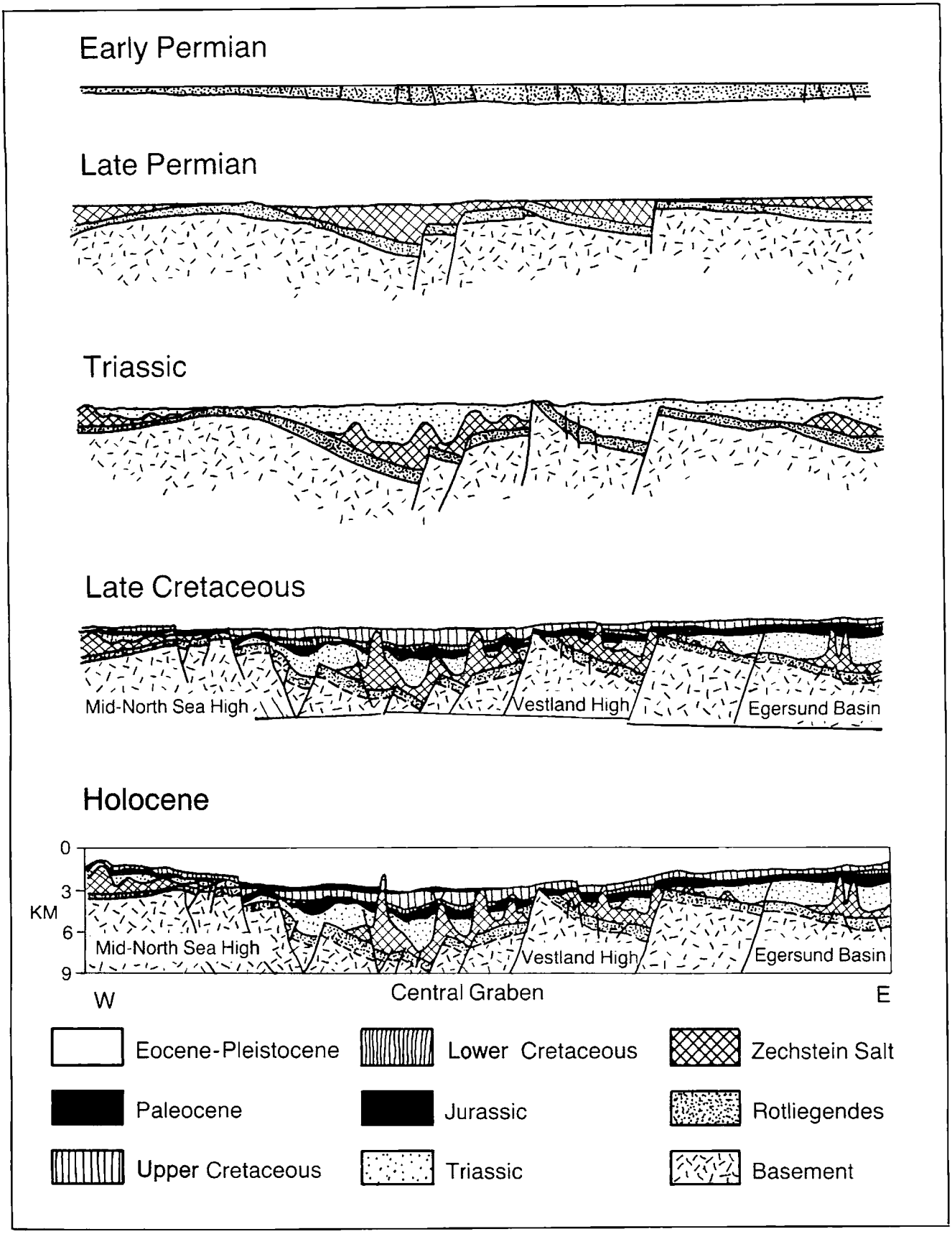


**Figure 8—Palinspastically restored cross section through Central graben (profile E of Figure 1). Unrestored section (Holocene) is from Ziegler (1978).**

from fault-controlled to regional subsidence is dated as Albian to Aptian (Kent, 1976). Major periods of normal faulting also were absent during the mid-Triassic through Early Jurassic, and during the Early Permian (Ziegler, 1982).

Thus, the history of the Central graben area appears to alternate between periods of localized graben formation and periods of regional basin subsidence. Rifting stages since the Permian are most likely the Late Permian through Early Triassic, the mid-Jurassic through earliest Cretaceous, and, tentatively, the Quaternary.

Crustal extension models, as discussed earlier, predict a period of regional subsidence following each rifting event. In this respect, the models match well the observed alternation of subsidence styles in the Central graben area. Early modeling studies (Beaumont, 1978; Sclater and Christie, 1980; Donato and Tully, 1981) included only one Jurassic/Cretaceous event. Wood and Barton (1983) recognized two phases of extension in Central graben evolution. J. C. Sclater and J. O. Salvesen (1987, personal communication) consider a third earlier phase in the Carboniferous. Unfortunately, the more phases of extension that are included, the more poorly constrained are estimates of the timing and magnitude of extension during the various rift phases. Therefore, we must look at the other evidence for crustal extension within the Central graben.

### Basement Extension

In basins dominated by crustal extension, total extension on basement faults, E (measured in kilometers), and tectonic subsidence, $V_T$ (measured in cubic kilometers per unit length of rift), are related by equation 5. We have used this relationship in the Central graben area by estimating E and $V_T$ between 54 °N and 58 °N. The total extension is obtained by mapping the fault planes of major Central graben faults. The total east-west extension of the basal Zechstein across the North Sea is estimated at every one-quarter degree of latitude as shown in Figure 9a. A discussion on the accuracy of this procedure is given in Appendix 2. The volume of tectonic subsidence is estimated from Figure 6a and b. Figure 9b shows the ratio of predicted subsidence from equation 5 to observed subsidence from latitudes 54 °N to 58 °N. Maximum and minimum estimates of this ratio are used because of uncertainties in estimating the extension on normal faults (see Appendix 2).

Figure 9b shows that the percentage of extension accounted for by observed basement extension between latitudes 54 °N and 58 °N, within the bounds of error, is uniformly low, on the order of 10%. The tectonic subsidence north of 56 ° includes the Norwegian-Danish basin (see Figure 1). This basin adds significantly to the total tectonic subsidence but not to our estimates of east-west extension across major basement faults. These results suggest that other mechanisms of basin formation have contributed to subsidence in this area, particularly within the Norwegian-Danish basin.

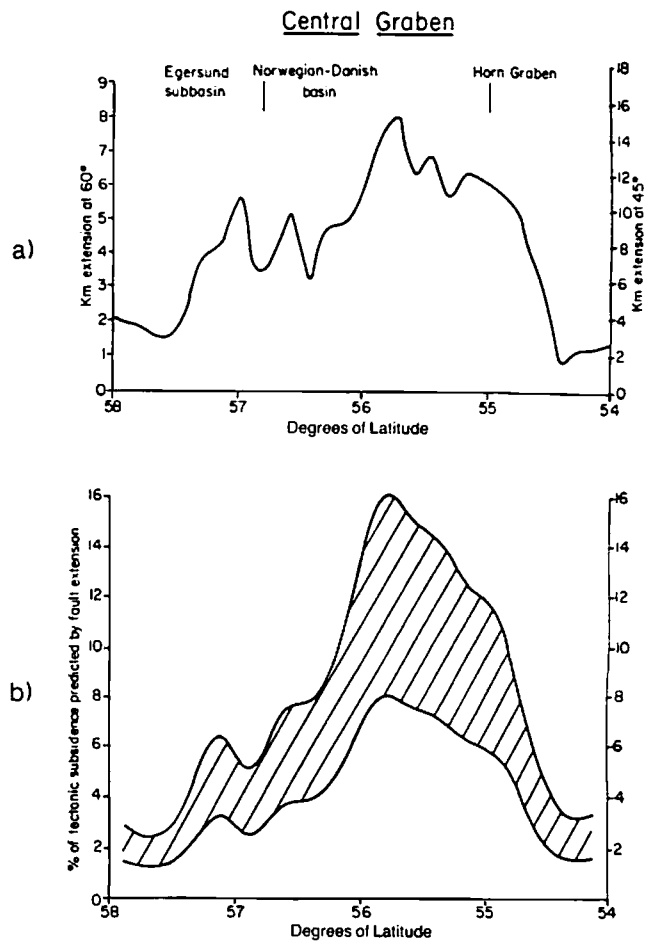


**Figure 9—(a) Total extension as function of latitude in Central graben. Two scales are given depending on assumed average dip at base Zechstein level of major faults accommodating extension. Reconstruction of faults is based on structure contour maps of Day et al (1981), published cross sections listed in Figure 1, and average dip angle on major faults from Blair (1975), Gibbs (1983), and Halstead (1975). See Appendix 2 for discussion of this procedure's accuracy. (b) Ratio of predicted subsidence from equation 5 to observed subsidence from latitudes 54 °N to 58 °N. Maximum and minimum range is placed on estimates of this ratio because of uncertainties in estimating extension on normal faults (see Appendix 2). Percentage of extension accounted for by observed basement extension is uniformly low.**

### Crustal Structure

The amount of extension across the Central graben should be reflected in shallow depths to the M-discontinuity beneath the rift. Seismic reflection and refraction profiling has been carried out by Christie and Sclater (1980) across the Witch Ground graben (line KK in Figure 1) and the Central graben (Barton and Wood, 1984). The profile across the Central graben (line LL in Figure 1) shows significant elevation of the M-discontinuity particularly in narrow region close to the graben axis (Figure 10). The volume/linear length of rift of the relief of the M-discontinuity, M, and tectonic subsidence, $V_T$, across this section are approximately 800 and 1,000 km$^2$, respectively. The crustal extension model

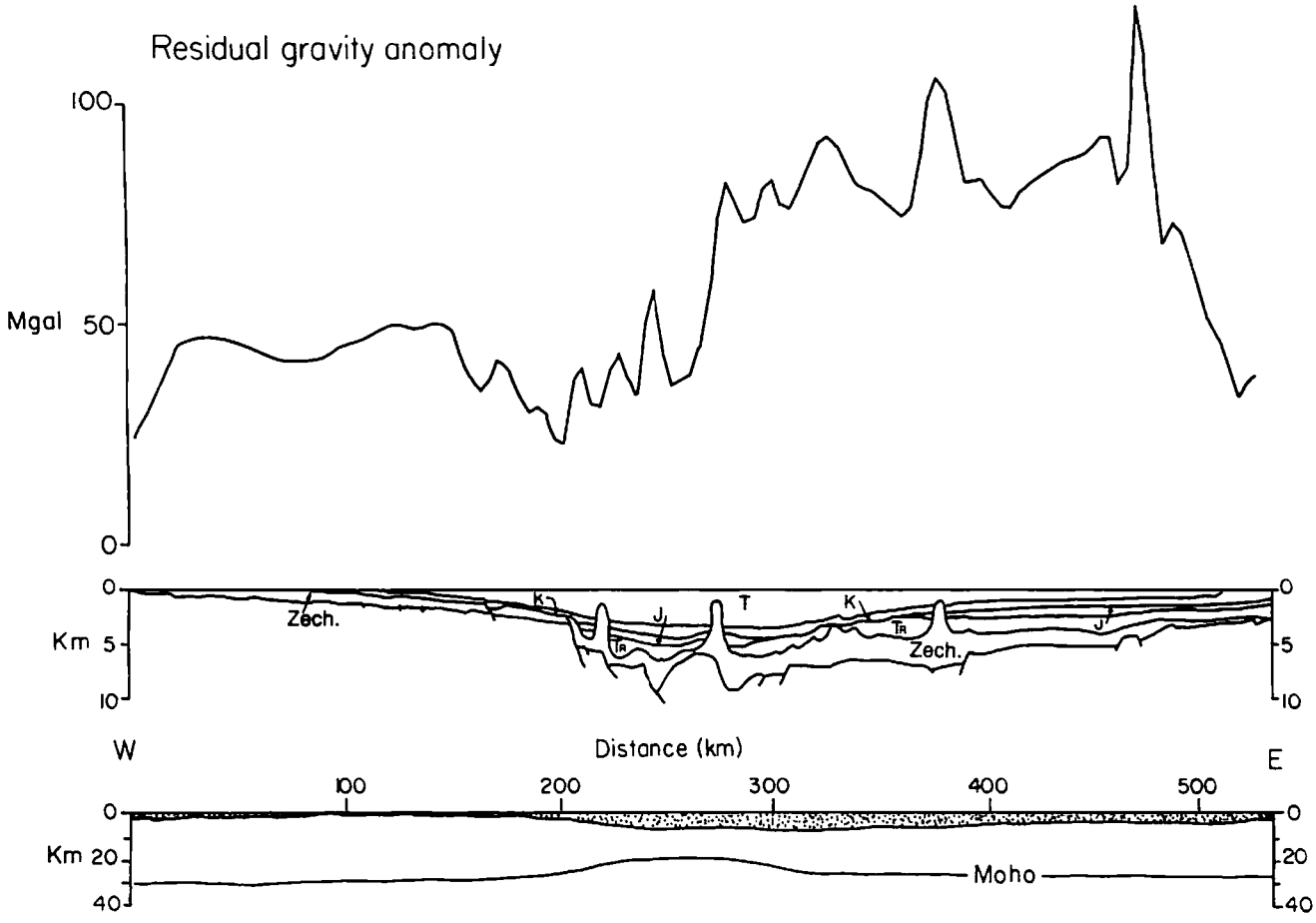


**Figure 10—Residual gravity over Central graben refraction line (Barton and Wood, 1984) obtained by correcting observed free-air gravity for gravitational attraction of sediments (density and porosity as determined by Appendix 1 method), and M-discontinuity topography. Resulting anomaly is strongly positive, suggesting deep crustal positive density anomalies are present, particularly in eastern part of cross section. Refraction velocities obtained by Barton and Wood (1984) also support this variation in crustal structure. Zech. = Zechstein.**

from equation 8 predicts far less tectonic subsidence for the observed Moho topography. This result suggests that other causes for basin tectonic subsidence may also be important in the evolution of the central region of the North Sea.

The refraction seismic interpretation of Barton and Wood (1984) shows significant variations in velocity structure consistent with large changes in crustal density from west to east across the Central graben. Figure 10 shows a residual gravity anomaly profile across the Central graben along the seismic refraction line obtained by correcting the observed free-air gravity anomaly for the effects of changes in water depth, sediment load, and the M-discontinuity. This anomaly, therefore, reflects lateral density distributions in the crust and upper mantle that cannot be explained in terms of undulations of the M-discontinuity.

### Form of Post-Jurassic Subsidence

Various authors (Sclater and Christie, 1980; Wood and Barton, 1983; Barton and Wood, 1984) have suggested that the post-Jurassic tectonic subsidence of the Central graben can be largely accounted for by thermal cooling of the lithosphere following Jurassic rifting. The tectonic subsidence maps of Figure 6, however, do not approximate simple postrift thermal subsidence. The rate of tectonic subsidence within the graben area, from the Early Cretaceous to Pliocene, does not decline, as is typical of thermal subsidence, but, based on concavity index, remains nearly constant or accelerates (Figure 11).

The maps of Cretaceous and Tertiary tectonic subsidence (Figures 6a, b) show few periods of tectonic quiescence during postrift basin evolution. Major tectonic subsidence centers appear and disappear within relatively short periods, e.g., the Ergesund basin in the Late Cretaceous or the upper Central graben in the Miocene. As discussed earlier, the Quaternary appears to represent a new phase of basin subsidence. These results suggest that thermal subsidence is only one component of basin evolution during the Cretaceous and Tertiary of the Central graben.

### Flexural Rigidity

An estimate of the rigidity of the Central graben region has been obtained (Barton and Wood, 1984) by compar-

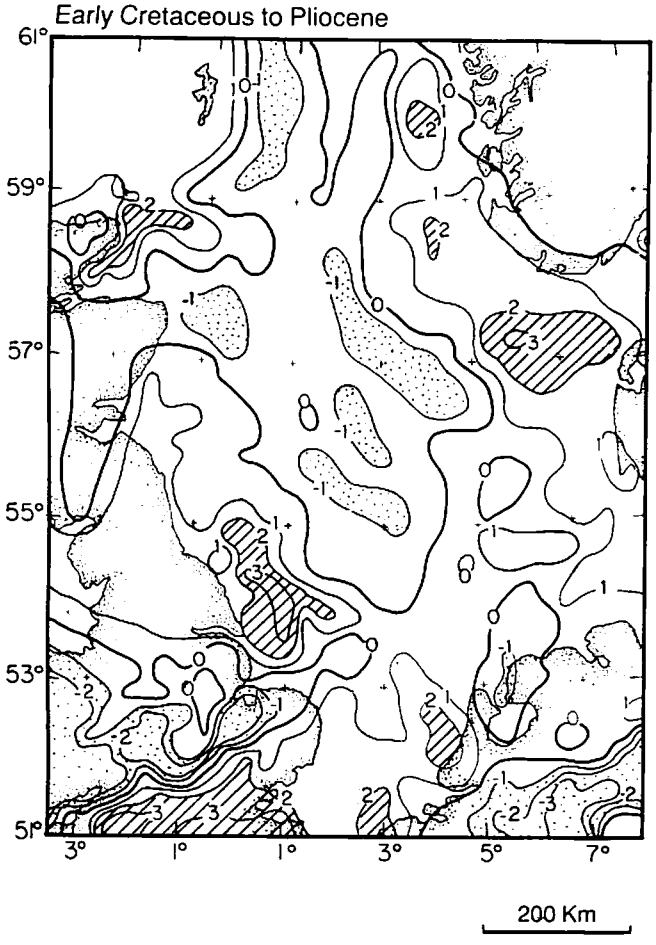


Figure 11—Regions of accelerating (dotted), decelerating (hatched), and nearly linear (unshaded) tectonic subsidence between Early Cretaceous and Pliocene, contoured at 10 × the concavity index C. Thermal subsidence hypothesis is rejected due to observed linear to accelerating subsidence in Central graben. Concavity index of accumulation function a(t) is defined in text.

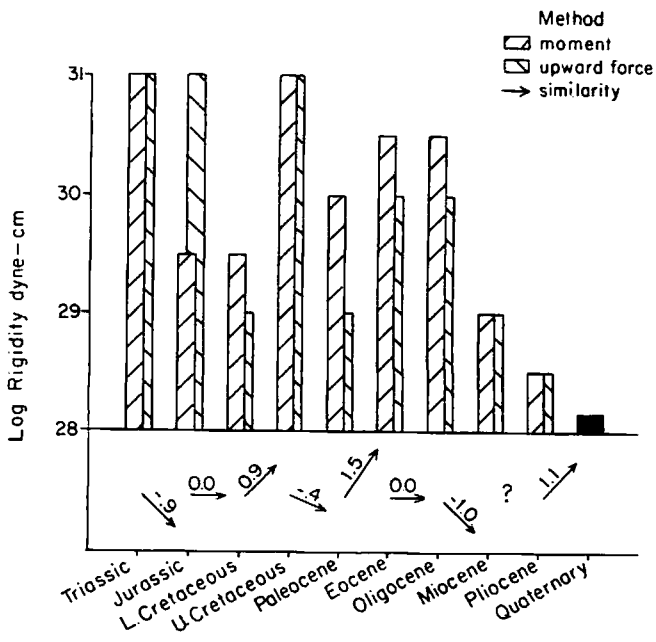


Figure 12—Determinations of rigidity for ten time-stratigraphic units. Quaternary rigidity is based on free-air gravity (see text). For other intervals, three determinations are shown. First determination (solid arrows) compares shape of succeeding units to determine relative change in flexural response from unit to unit. Histogram shows determinations by minimum moment and minimum upward force methods (see Appendix 3). These methods invert subsidence response of each unit for an applied flexural load. Assumed rigidity is lowered for each inversion until predicted load is of reasonable shape, i.e., load is concentrated at one or several depocenters (minimum moment) or has only small component acting in upward direction.

ing observed free-air gravity (derived from altimetry data) to modeled gravity for differing degrees of flexural compensation to the tectonic subsidence and sediment loading since the Cretaceous. The best-fitting value of D = $10^{28}$ dyne/cm (from equation 10) places the depth to the 450 °C isotherm 5 km below sedimentary basement B during or after the majority of sediment and tectonic loading. The effective rifting age to account for the observed rigidity from equation 11 is less than 20 m.y., a value not at all expected if the last thermal event in the Central graben occurred during earliest Cretaceous rifting.

One possible explanation, however, for the observed low rigidity is thermal rejuvenation of the Central graben during the late Cenozoic. To examine this possibility, we used load-shape analysis to estimate average flexural rigidity during the emplacement of ten increments of tectonic loading as amplified by sediment fill from the Triassic to the Quaternary. The results of this analysis by three different methods are shown in Figure 12 (see also Appendix 3). With the exception of the Quaternary, the derived rigidities show good agreement between the various methods. (We show in Appendix 3 that all three methods of load shape analysis most likely have failed to recover an accurate rigidity for the Quaternary.) The rigidity estimates (Figure 12) show a consistent decrease from the Upper Cretaceous through the Pliocene. The low rigidity value derived from the gravity study of Barton and Wood (1984) is consistent with this progressive lowering of flexural rigidity during the Tertiary. We suggest that thermal rejuvenation has led to ongoing isostatic reequilibration of the Central graben and thus, at the present time, nearly complete isostatic compensation. The low rigidity estimates from gravity studies probably reflect this last phase of reequilibration.

## VIKING GRABEN EVOLUTION

The Viking graben has long been recognized as a rift-type basin. Alvarez (1985), in a study of the subsidence of the northern North Sea between 59 °N and 62 °N, produced maps of tectonic subsidence for seven time/

stratigraphic intervals within the basin. The timing of major periods of fault movement in the Viking graben has been established by many writers working with seismic reflection profiles across the basin (Halstead, 1975; De'Ath and Schuyleman, 1981; Eynon, 1981; Gray and Barnes, 1981; Hallet, 1981; Harding, 1983). Figure 13 schematically illustrates the results of these studies. Three phases of extensional faulting can be distinguished in this figure: Early Triassic, mid-Jurassic through earliest Cretaceous, and latest Cretaceous through Paleocene.

### Triassic Subsidence

The Triassic phase of subsidence consists of a downdropped axial graben 50-km wide set within a broad basin of regional subsidence. Reconstruction of this section and others (Fisher, 1984; Glennie, 1984) shows approximately 20 km of basement extension across the Viking graben by normal faulting during the Triassic.

A comparison of predicted (using equations 3-5) and observed (from Alvarez, 1985) tectonic subsidence for the Triassic is given in Table 2. The observed value of tectonic subsidence is significantly larger than the predicted syn-rift subsidence, but approximately equal to the total predicted tectonic subsidence. This difference suggests that the postrift stage of thermal subsidence is an important component in Triassic subsidence. The observed basin stratigraphy is, in fact, quite similar to the two-dimensional extension models of narrow rift structures of Cochran (1983), which show that a significant percentage of thermal subsidence can take place during the rifting stage of a narrow graben system.

### Jurassic and Early Cretaceous Subsidence

By far the most fault extension across the Viking graben took place during the mid-Jurassic through Early Cretaceous (Figure 13). Characteristic fault-block geometry involves large rotation on normal listric faults and associated strike-slip movement (Halstead, 1975; Hay, 1978). Basement extension distributed across a 200-km wide rift basin averages approximately 45 km (estimated from cross sections from Eynon, 1981; Ziegler, 1982; Glennie, 1984; Fisher, 1984). The section shown in Figure 13 shows Early Cretaceous differential subsidence across major growth faults. Sections from the United Kingdom sector at 62°N (Vail and Todd, 1981), however, show strong phases of growth faulting in the mid-Jurassic.

A comparison of predicted (from equation 3) and observed (from Alvarez, 1985) tectonic subsidence during the mid-Jurassic through the Early Cretaceous is given in Table 2. The observed value of tectonic subsidence is approximately equal to the predicted syn-rift subsidence. This suggests that the mid-Jurassic/Early Cretaceous rifting phase in the northern North Sea can be largely accounted for by observed crustal extension during this period.

### Late Cretaceous and Tertiary Subsidence

Various writers (Donato and Tully, 1981; Dimitropoulos and Donato, 1982; Alvarez, 1985) have suggested that Late Cretaceous and Tertiary subsidence of the northern North Sea can be largely accounted for by thermal cooling of the lithosphere following or during rifting. The concavity of tectonic subsidence between the Paleocene and the Pliocene, correcting for eustatic sea level changes (Figure 14), ranges between 0.2 and 0.4 within the Viking graben, consistent with a thermal cooling origin for subsidence during this period. Unfortunately, the concavity of tectonic subsidence within the Late Cretaceous cannot be assessed from the present data. With this limitation in mind, using 0.3 from Figure 14 as the average concavity of postrift subsidence in equation 7 places the start of thermal subsidence at 121 Ma (within the Early Cretaceous).

### Quaternary Subsidence

The tectonic subsidence map of the Quaternary (Figure 6a) shows an elongate riftlike form on the eastern flank of the Viking graben. Possible Quaternary rifting is also indicated by present-day seismicity (Browitt and Newmark, 1981), which shows larger than normal magnitude events associated with the margins of strong Quaternary subsidence.

### Crustal Structure and Flexural Rigidity

The amount of crustal extension across the Viking graben can be determined from the elevation of the M-discontinuity beneath the rift. The 2,000 $km^2$ (volume/linear length of rift) of Moho topography above 30 km, M, is observed on the refraction profile of Solli (1976) across the Viking graben (line JJ in Figure 1). The predicted total volume/linear length of rift of tectonic subsidence from equation 8 is 700 $km^2$ and is derived from

$$M(2{,}000\ km^2) = 2.83 \cdot V_T(700\ km^2).$$

The crustal extension model is strongly supported, therefore, by the approximate agreement between this result and the estimated observed total tectonic subsidence of 510 $km^2$ (Table 1).

An estimated rigidity for the Viking graben of $D = 10^{30}$ dyne/cm is obtained by comparing observed free-air gravity (Figure 15) to modeled gravity for differing degrees of flexural compensation to the tectonic subsidence and sediment loading since the Triassic. By substituting this value into equation 10, the depth to the 450°C isotherm is predicted to be 22 km below sedimentary basement B. The effective rifting age to account for the observed rigidity, with B equal to 8 km from equation 11, is 117 Ma (within the Early Cretaceous). Thus, the observed rigidity of the Viking graben is consistent with a

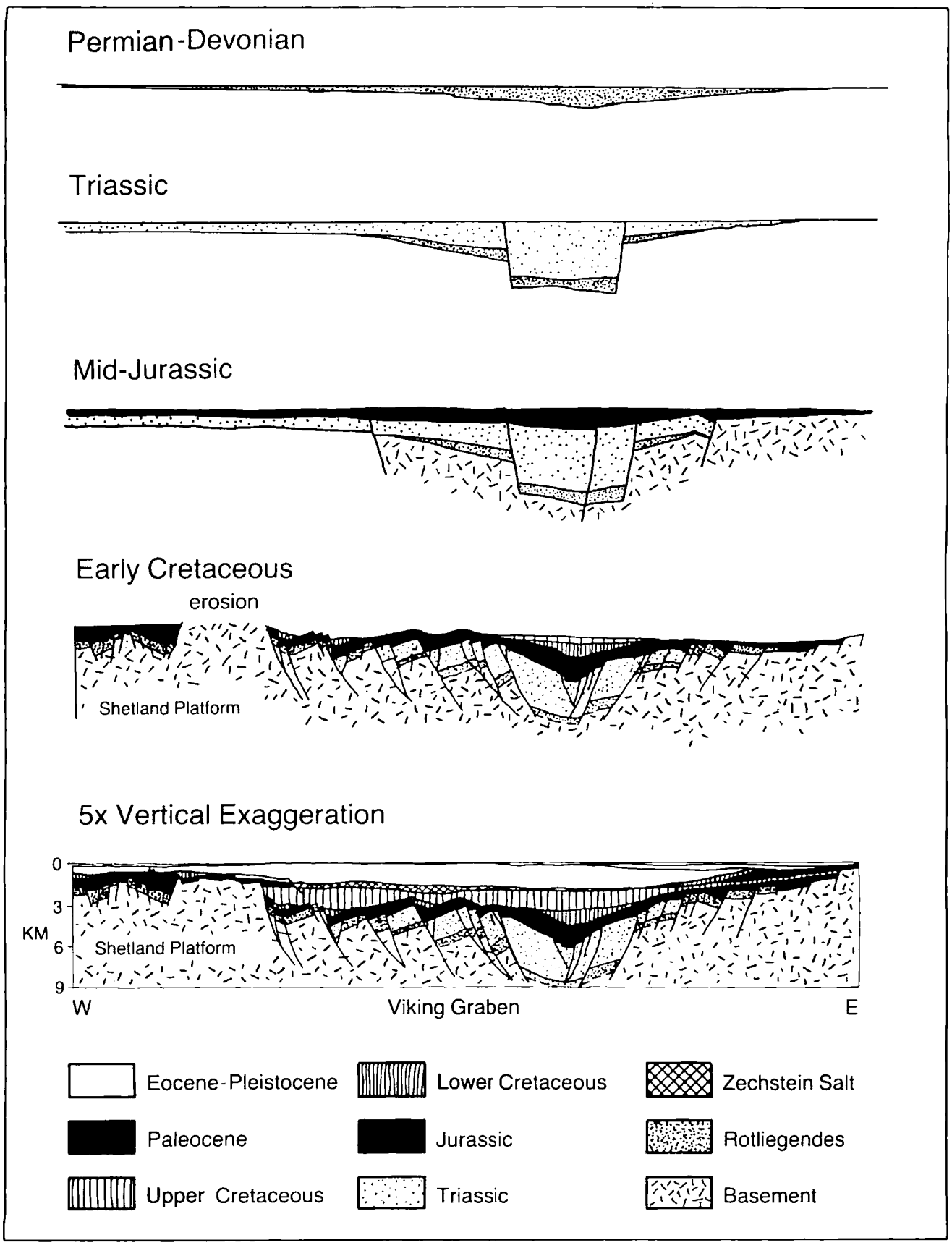


**Figure 13—Palinspastically restored cross sections through Viking graben (profile A of Figure 1). Unrestored section is from Ziegler (1978).**

Table 2. Northern North Sea: Extension vs. Tectonic Subsidence

| | E (km) (observed) | $V_1$(km$^2$) (from eq. 3) | $V_2$(km$^2$) (from eq. 4) | $V_T$(km$^2$) (from eq. 5) | V(km$^2$) (observed) |
|---|---|---|---|---|---|
| Triassic | 20 | 70 | 90 | 160 | 180 |
| Mid-Jurassic/Early Cretaceous | 45 | 160 | — | — | 130 |
| Total | 65 | — | — | 500 | 510 |

Late Jurassic/earliest Cretaceous rifting phase in which crustal extension within the graben played a dominant role.

### Quaternary Rejuvenation

Our analysis of northern and southern North Sea subsidence indicates that the Quaternary was a period of anomalously high rates of regional tectonic subsidence associated with anomalously low values of flexural rigidity.

Depocenters of Quaternary subsidence apparently reactivated earlier trends. Features present in both the Quaternary and Lower Cretaceous, for example, include differential subsidence of the West Netherlands basin, Egersund subbasin, Horda platform, and Central graben as well as differential uplift of the English subbasin.

One possible explanation for Quaternary subsidence is that the Quaternary formed in response to regional heating, allowing isostatic reequilibration of previously applied (e.g., Lower Cretaceous) sediment and lithospheric loads. The magnitude and extent of thermal rejuvenation should be reflected in regional maps of heat flow, gravity, and present-day flexural rigidity.

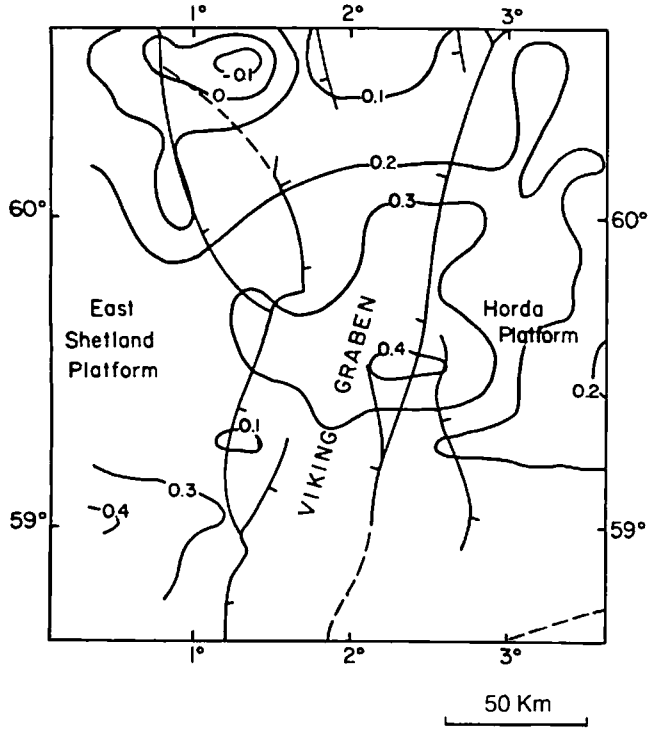


Figure 14—Concavity index of tectonic subsidence between Paleocene and Pliocene in northern North Sea as in Figure 11. Eustatic sea level correction has been added to tectonic subsidence using sea level curve of Watts and Thorne (1984). Observed concavity supports thermal subsidence hypothesis.

A heat-flow map of the North Sea (Figure 16) has been prepared based on published information on geothermal gradients and borehole temperatures (Cornelius, 1975; Norwegian Petroleum Directorate, 1976; Carstens and Finstad, 1981). The variation of heat flow shown in Figure 16 agrees well with the work of Andrews-Speed et al (1984) in the western North Sea. These writers showed that heat flow is significantly different above and below the upper kilometer of sediments. Their variation of heat flow below the upper kilometer of sediments agrees substantially better with the heat flow given here (Figure 16).

The pattern of Quaternary tectonic subsidence (Figure 6a) appears to correlate with variations of heat flow (Figure 16). The West Netherlands basin, the lower and upper Central graben, the eastern flank of the Viking graben, and Horda platform are all Quaternary subsidence centers and heat-flow highs. However, a heat-flow high at ≈54 °N 2 °E (English subbasin) is associated with a local minimum of Quaternary subsidence. Barnard and Cooper (1983) suggested that the stratigraphy of the English subbasin indicates a recent phase of structural inversion (uplift) since the latest Pliocene.

The association of differential Quaternary subsidence or uplift with areas of anomalously high heat flow suggests that the Quaternary is a period of active thermal rejuvenation. Depending on the tectonic setting, thermal heating is apparently associated with either accelerated subsidence or structural inversion. Further support for this tectonic interpretation comes from an analysis of North Sea gravity data.

Figure 15 shows a free-air gravity anomaly map of the North Sea basin compiled using available submarine (Collette, 1960) and surface-ship measurements. Much of the short wavelength energy in the free-air gravity of the North Sea is probably caused by granitic and mafic plutonic intrusions (Collette, 1960; Donato and Tully, 1982). Threlfall (1981) showed the location of basic igneous intrusions identified on the basis of aeromagnetic surveying in the central and northern North Sea. Four of these proposed bodies can also be identified on the free-air gravity anomaly map of Figure 15.

Intermediate wavelength (>50 km) gravity anomalies are generally associated with flexural compensation of surface loads (e.g., McKenzie and Bowin, 1976; Karner, 1982). For gravity anomalies over a sedimentary basin, a measure of the load is provided by the total deflection of the crust by the weight of the sediments. A matrix relationship between the intermediate wavelength compo-

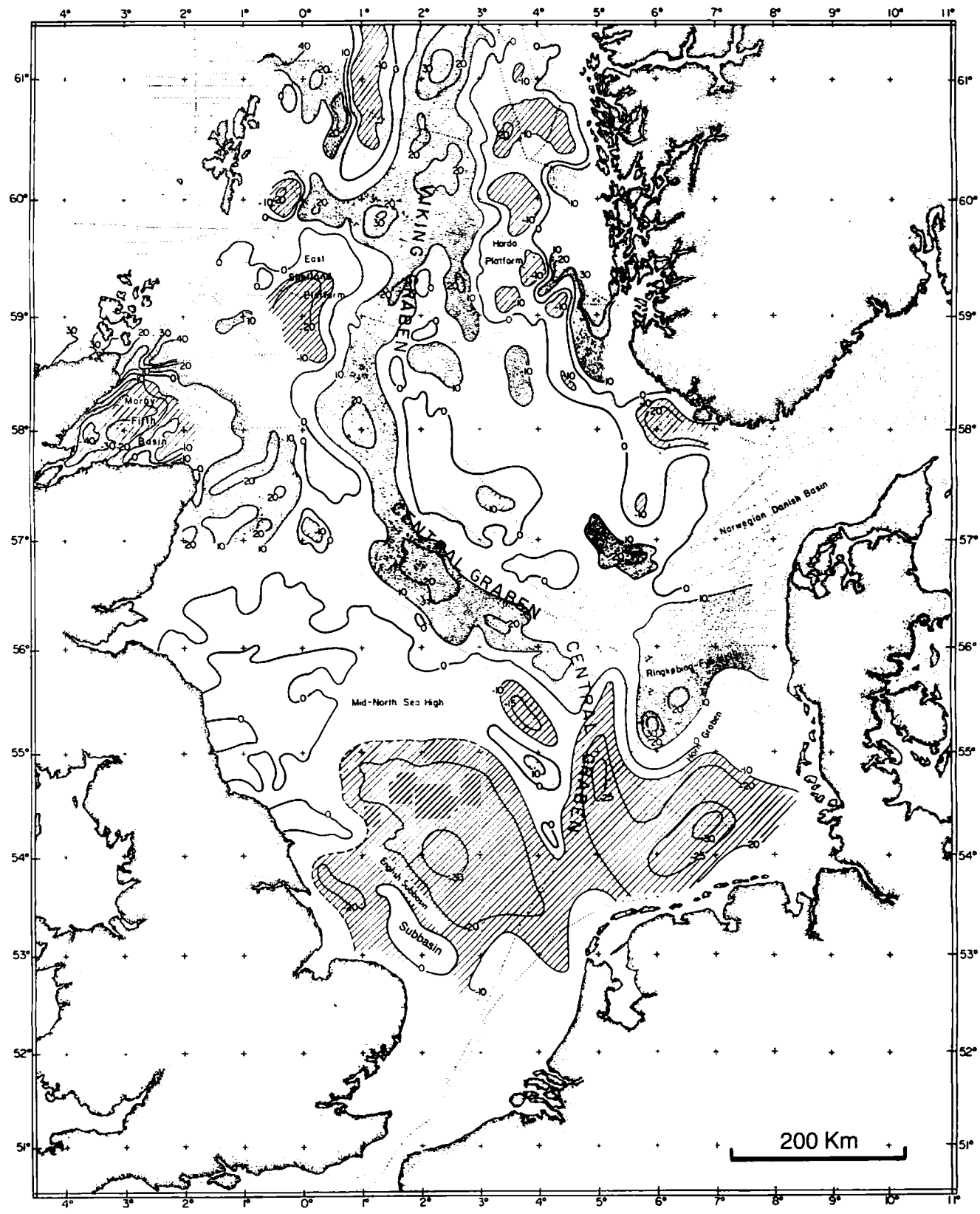


Figure 15—Free-air gravity anomaly map of North Sea contoured at 10-mgal intervals. Gravity measurements (shown as dotted lines) have been compiled from Lamont-Doherty Global Gravity Data Bank supplemented by other published maps in the Dutch North Sea (Strang van Hess, 1981), Moray Firth (I.G.S. of Britain map series), and southern North Sea (Day et al, 1981). Proposed basic intrusions are located at 62 °N 0 °15 'E, 60 °N 1 °30 'E, 58 °30 'N 2 °W, and 56 °30 'N 2 °E.

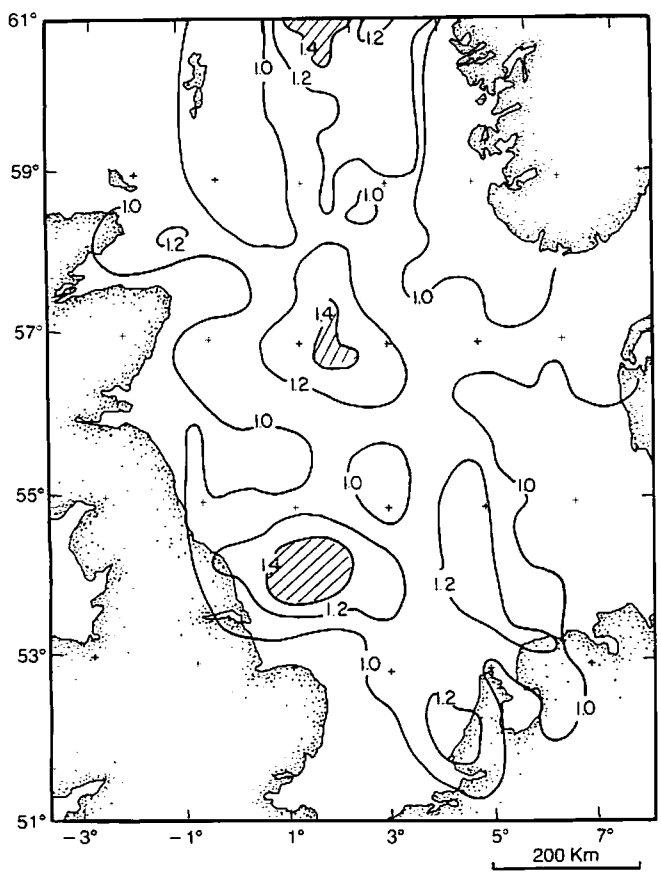


Figure 16—Basement heat flow contoured at 0.2 HFU determined from borehole temperature gradients (largely from Cornelius, 1975; Carstens and Finstad, 1981). Borehole temperatures were increased by 15% to approximately counteract the cooling due to mud circulation. This approximation is appropriate to mean circulation time of 10 hr (Carstens and Finstad, 1981). Heat flow is given by average temperature gradient multiplied by average thermal conductivity. Thermal conductivity was assumed to range linearly between 0.0015 cal $°C^{-1}cm^{-1}sec^{-1}$, the conductivity of water, and 0.005 cal $°C^{-1}cm^{-1}sec^{-1}$, conductivity of grains, depending on porosity.

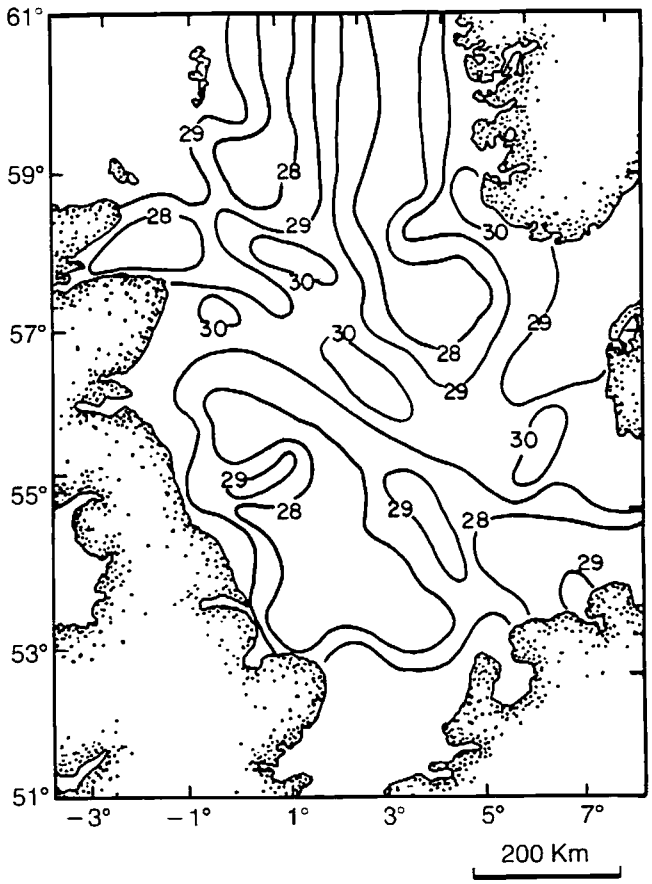


Figure 17—Present-day flexural rigidity derived from inversion of gravity and total tectonic subsidence. Contours are as follows: 28 = $10^{28}$ dyne/cm, 29 = $10^{29}$ dyne/cm, etc. Variation of rigidity is reflection of thermal rejuvenation during Neogene and Quaternary.

nent of free-air gravity and the depth to basement obtained by Thorne (1985) can be used to invert for flexural rigidity and its spatial variation in plan view.

The variation of present-day flexural rigidity across the North Sea derived from this inversion technique (Figure 17) shows, as expected, low values of flexural rigidity associated with areas of higher than average heat flow. Areas with high values of flexural rigidity, however, are associated with lower heat flow. The troughlike form of maximum Quaternary subsidence in several places deviated around crustal blocks of high flexural rigidity. A rigidity high of $10^{31}$ dyne/cm in the lower Central graben, for example, remained a relatively positive feature during Quaternary subsidence.

Both gravity and heat-flow data in the North Sea suggest that thermal rejuvenation with associated reduction of flexural rigidity played a role in Quaternary subsidence. The similarity of the form of Quaternary subsidence with other time intervals, particularly the Early Cretaceous, suggests a reactivation of previous tectonic loading centers.

The progressive lowering of flexural rigidity during the Cenozoic (Figure 12) and the tectonic subsidence during this period suggest that thermal rejuvenation and tectonic reactivation began early in the Tertiary. The Quaternary, in this context, represents a culmination of this tectonic phase. However, a geophysical model quantitatively relating thermal rejuvenation to tectonic reactivation remains to be developed.

## DISCUSSION

### Implications for Rift Models

The question arises as to whether the contrasting rift styles of the northern and southern North Sea can partially be explained by fundamental differences inherited from their Caledonian and Variscan stages of development. The crystalline basement of the northern North Sea consists mainly of high-grade metamorphic rocks of a northeast-trending branch of the Caledonides, and the basement of the southern North Sea is formed by a gener-

ally low-grade (greenschist facies in samples recovered from wells) east-west-trending branch of the Caledonides (Frost et al, 1981; Ziegler, 1981). These differences in underlying metamorphic grade and structural grain may have been one controlling factor in the post-Paleozoic evolution of the North Sea. Several writers have suggested, for example, a control of northern North Sea rift structures by the grain of the underlying Caledonian basement (Blair, 1975; Halstead, 1975; Ziegler, 1975; Johnson and Dingwall, 1981; Threlfall, 1981). In the southern North Sea, however, regional linear fracture zones, graben boundary faults, and inversion axes appear to be affected by a northwest Variscan structural trend (Dikkers, 1977; Glennie,1984).

Falvey (1974) and Middleton (1980) have suggested that deep-crustal metamorphism may be the cause for a large part of the tectonic subsidence of a passive margin or intracratonic basin. The northern North Sea, underlain by high-grade Caledonian basement, is clearly not a candidate for this subsidence mechanism. This mechanism, however, may have contributed to subsidence of the southern North Sea during Cenozoic thermal rejuvenation of the area. The time history of subsidence due to crustal metamorphism would be affected by such poorly known factors as (1) the kinetics of the limiting metamorphic reactions, (2) the net volume change of the reaction greenschist ↔ amphibolite + water, and (3) how long metamorphic fluids takes to percolate from within the crust to the surface of the basin.

During the Late Carboniferous, the southern North Sea became a foreland to the Variscides farther to the south. Recent studies of the Hercynian (Variscan) orogen indicate a regime dominated by a complicated interplay of extensional, compressional, and wrench tectonics coupled with regional thermal metamorphism, associated uplift, erosion, and basic volcanism (Dewey, 1982; Ziegler, 1984; Wickham and Oxburgh, 1985). The evolution of the continental crust of the southern North Sea during this period may involve the intrusion of large volumes of basic magma into the lower part of the continental crust (McKenzie, 1984; Jowett and Jarvis, 1984; Ziegler, 1984). One component of subsidence in the southern North Sea may involve, therefore, the progressive transformation of crustal gabbro to eclogite. Fowler and Nisbet (1984) suggested that either prolonged (>100 m.y.) or initially rapid tectonic subsidence can be caused by such an intrusion depending critically on the temperature/time history of the emplaced mafic body.

The large lateral changes in crustal-density structure across the Central graben inferred from the refraction study of Barton and Wood (1984) also indicate that density changes associated with greenschist → amphibolite and basalt → ecogite metamorphism may be important crustal processes. To a certain degree, variations in density structure may be inherited from Caledonian and Hercynian crustal evolution. However, the fact that these variations compensate, to a large part, the continuing tectonic subsidence of the southern North Sea (Figures 6, 10) indicates that crustal-density changes have been an ongoing process.

Ziegler (1982, p. 101), speculating as to the cause of several distinct cycles of rifting in the basins of western and central Europe, suggested a fundamental control by periods of anomalously active aesthenospheric convection. During such periods, in his view, mantle convection exerted a tensional rift-forming stress on the overlying plate, and at the same time, the ascent of hot aesthenospheric material to the crust-mantle boundary caused the upward displacement of the crust-mantle boundary by "thermally-induced physico-chemical processes" affecting the lower crust.

Unfortunately, the qualitative model of Ziegler (1982) is hard to test on a quantitative basis. A first attempt to model the suggested processes was made by Thorne (1985). This numerical model examined the subsequent basin evolution after a short-lived period of anomalously active aesthenospheric convection by adding the effects on tectonic subsidence of crustal/lithospheric stretching, densification due to greenschist-amphibolite and basalt-ecologite metamorphism, and heating and cooling within the aesthenosphere. Although the modeled stratigraphy (Figure 18) resembles similar cross sections through the Central graben, the many unknown parameters needed to quantitatively specify these effects render any predicted stratigraphy rather nondescript.

### Predicting Thermal Maturation

Geophysical basin subsidence modeling is often attempted to predict the timing and extent of source rock maturation (e.g., Royden et al, 1980; Sclater and Christie, 1980; Nunn et al, 1984; Watts and Thorne, 1984; Guidish et al, 1985). Welte et al (1983) described an integrated three-dimensional numerical model incorporating fluid flow, tectonic basin modeling, and organic geochemistry to predict hydrocarbon maturation. The question, however, for basin modelers is whether sophisticated models can avoid the inherent uncertainties involved in predicting temperature and maturation history.

The North Sea is in many ways an ideal basin for maturation modeling. Dominant source rocks for major oil fields have been identified (Barnard and Cooper, 1981, 1983; Cornford, 1984) and are few in number (i.e., the Kimmeridgian Clay for the Viking and Central grabens and the Westphalian Coal Measures for the southern gas fields). Moreover, the clear association of hydrocarbon-prone areas and burial depth of the Kimmeridgian (Cornford, 1984) suggests that vertical rather than lateral migration has been the main path for generated oils.

Model fits to maturation data in the North Sea have been achieved without burial-history compaction corrections (Mackenzie and McKenzie, 1983; Rønnevik et al, 1983) using constant or variable heat flow (Goff, 1983), and time-independent maturation (Fisher and Miles, 1983). Goff (1983), for example, matched vitrinite reflectance in the Viking graben either by a model allowing for heat-flow variations given by the crustal-extension model of McKenzie (1978) or by a model using constant heat flow with time. In either case, a recalibration of the rela-

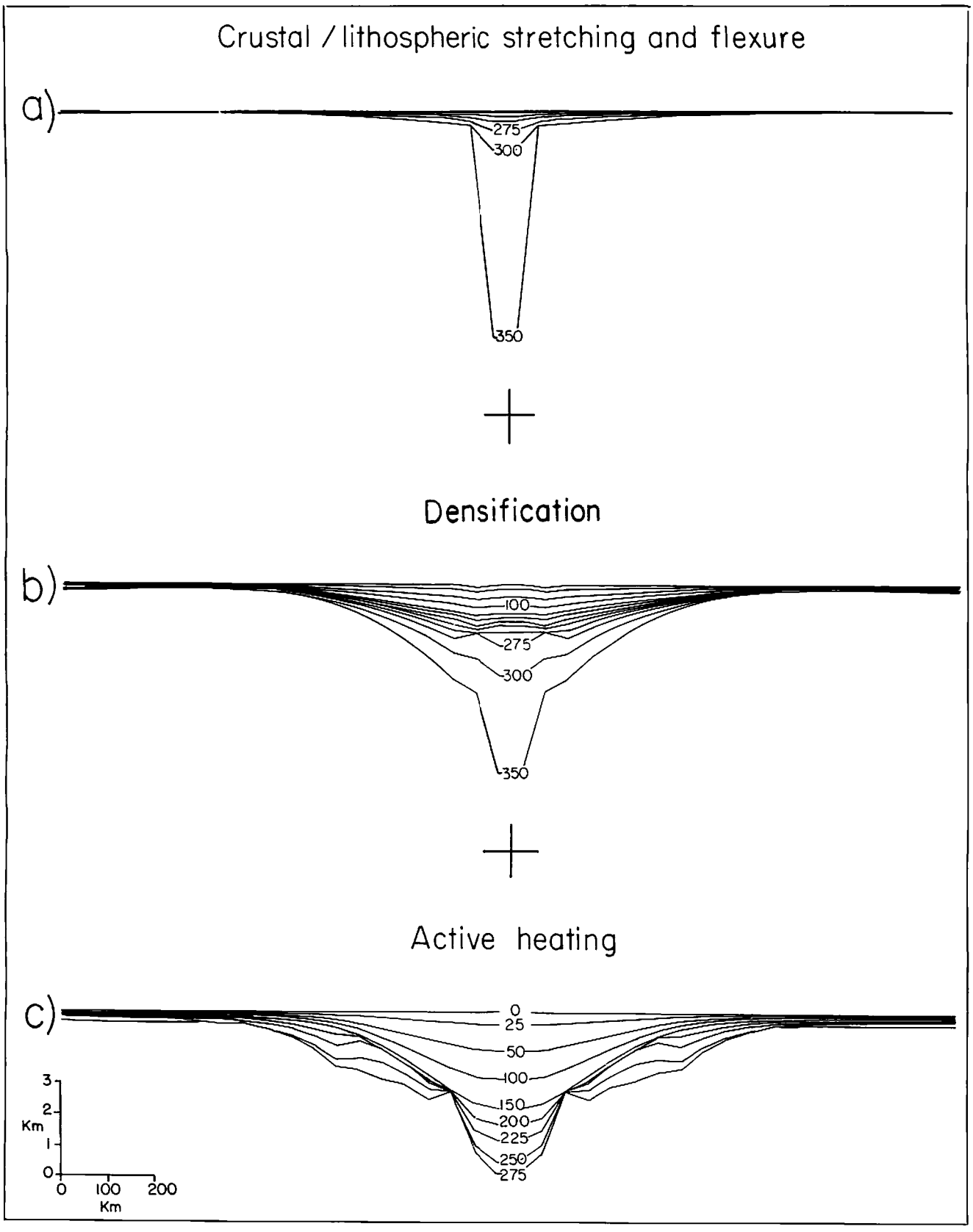


**Figure 18—Model basins for southern North Sea assuming (a) stretching and flexure, (b) basalt/eclogite and greenschist/amphibolite densification reactions, and (c) stretching, flexure, densification and active heating by asthenospheric convection. Time lines are labeled in m.y. Complete description of numerical model used in these simulations is given in Thorne (1985).**

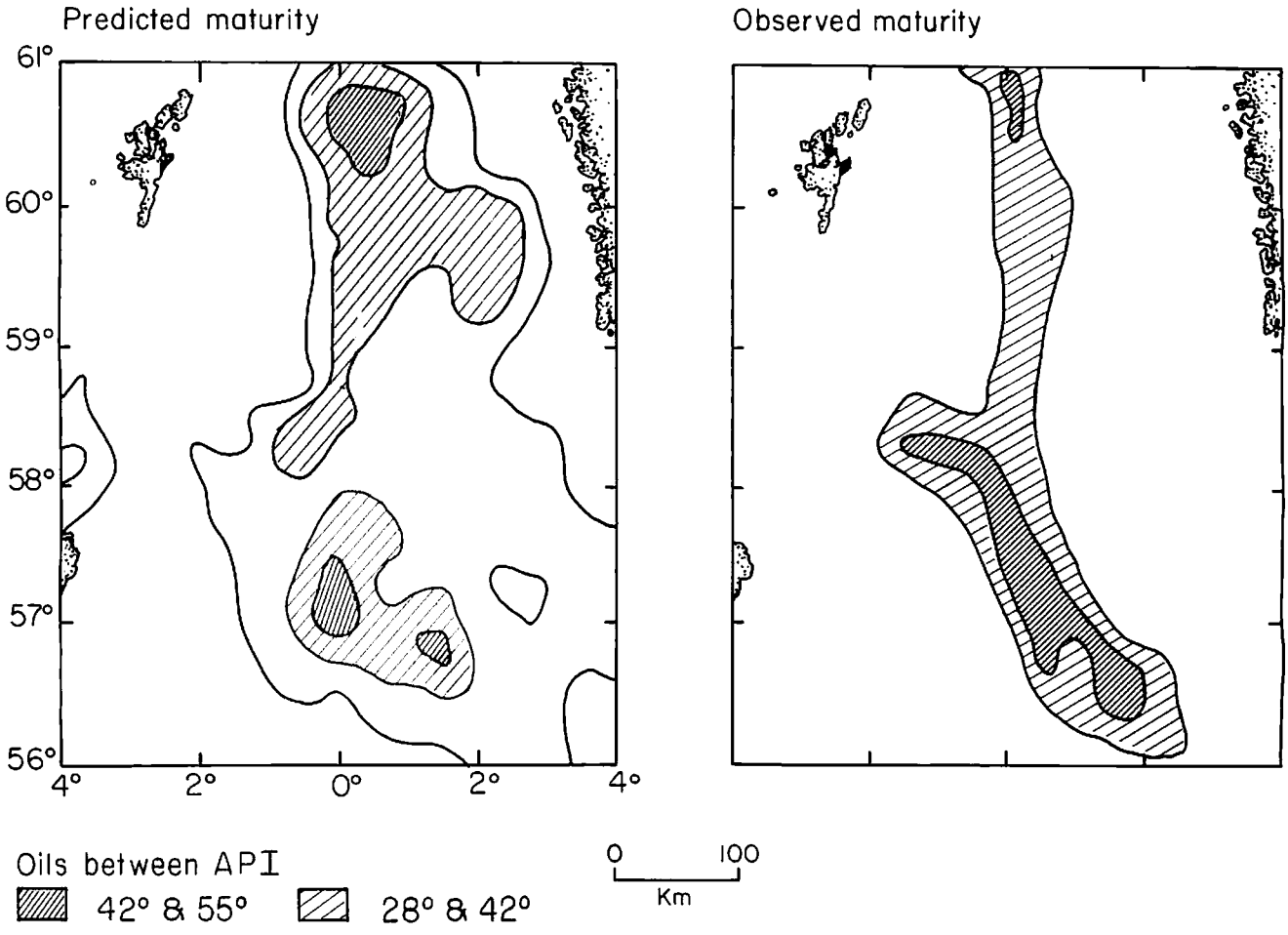


**Figure 19—Predicted and observed maturity of Upper Jurassic rocks shown as contours of oil gravity (API gravity). Observed maturity is after Barnard and Cooper (1981) and is based on recovered hydrocarbons. Predicted maturity is calculated from our model using a technique commonly used in conjunction with backstripping studies (Royden et al, 1980) assuming that heat flux is constant with time as shown in Figure 16.**

tionship between computed maturation index and vitrinite reflectance allowed for a good fit to the maturation data. We have repeated this experiment in the southern and northern North Sea based on our mapped variations of heat flow, subsidence history, and compaction coefficients (Figure 19). Computed values of Lopatin's maturation index are used to predict the generation of oils of various grades based on the calibration of Waples (1980). Within the uncertainty of model parameters, however, neither a constant nor variable heat-flow model can be ruled out on the basis of the present-day distribution of oils of varying grades.

The apparent ability of simple and sophisticated models alike to match maturation data indicates the need for model calibration on a test data set followed by rigorous testing of model predictions on data in other areas. Almost any model, simple or complicated, generally can be calibrated to (made to fit) the maturation data at one or several wells. The most geologically correct model should best be able to predict the expected variation of maturation away from the well used for calibration.

For example, Quaternary thermal rejuvenation, as suggested earlier, may have significantly altered the variation of heat flow across the North Sea. Quaternary variations should, however, have only a small time-integrated effect on the present maturity of buried source rocks and no effect on the distribution of mature hydrocarbons that have migrated from depth in the Tertiary. Some suggestion of this effect is seen in the data of Mackenzie and McKenzie (1983) on aromatization of hydrocarbons (Figure 20).

The Norwegian Sea north of the Viking graben is currently a frontier basin of active exploration interest. High Quaternary subsidence rates in the Møre and Vøring basins of the Norwegian margin (Bøen et al, 1984; Bukovics et al, 1984) suggest the possible extension of Quaternary thermal rejuvenation into this area. Maps of sub-Quaternary burial depth of potential source rocks, therefore, may be better indicators of potential maturity than present burial depth.

## SUMMARY

In this study, we investigated aspects of basin subsidence in the southern and northern North Sea through a

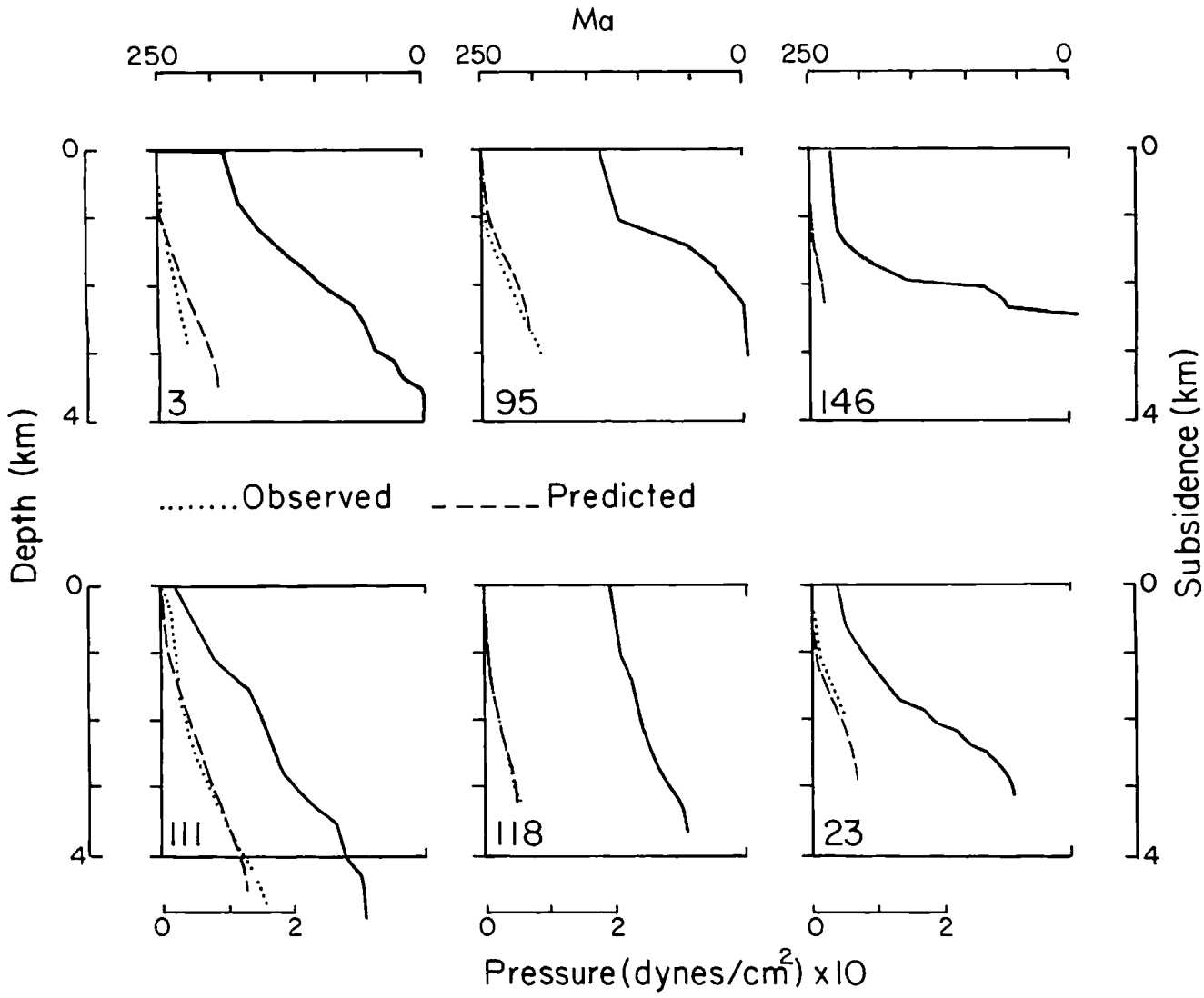


**Figure 21—Subsidence, observed and predicted overpressure for six North Sea wells. Well numbers are as in Figure 3. Observed overpressure is determined from integration of drilling-mud weight with depth. Predicted overpressure is determined by one-dimensional porous flow model as described in text. Solid line = subsidence, dotted line = observed overpressure, dashed line = predicted overpressure.**

quantitative analysis of tectonic subsidence and other geophysical data in these areas. An important stage in the analytical procedure is determining the compaction coefficients relating porosity to effective pressure from downhole geophysical information and numerical modeling of the development of sediment overpressures. Several conclusions can be reached from the data presented.

In northern areas of the North Sea, a multistage rifting history dominated by processes involving crustal/lithospheric stretching is largely responsible for the tectonic subsidence. Observed basement fault extension, crustal thinning, present-day flexural rigidity, and tectonic subsidence are predicted well by a simple stretching model of basin formation with rifting phases during the Triassic and mid-Jurassic–Early Cretaceous.

In southern areas of the North Sea (e.g., the Central graben), crustal stretching appears to play a less important role. The observed basement fault extension, crustal structure, time history of flexural rigidity, and tectonic subsidence suggest that other rift-related processes have contributed significantly to basin evolution. Possible additional mechanisms include the effects of anomalously active asthenospheric convection coupled with basalt-eclogite and deep crustal dewatering reactions.

Tectonic reactivation of the North Sea appears to be taking place in the Neogene and, to a greater extent, in the Quaternary. The importance of thermal rejuvenation during this phase is borne out by the association of areas of differential subsidence with high heat flow and low flexural rigidity. One component of tectonic reactivation may be due to thermally induced isostatic reequilibration of older tectonic loads. However, the troughlike form of Quaternary tectonic subsidence suggests a new phase of rifting may be starting in the North Sea. Similar Quaternary reactivation also occured in the Møre and Vøring basins of the Norwegian margin. Recognition of this phase of tectonic development may significantly affect exploration in these areas.

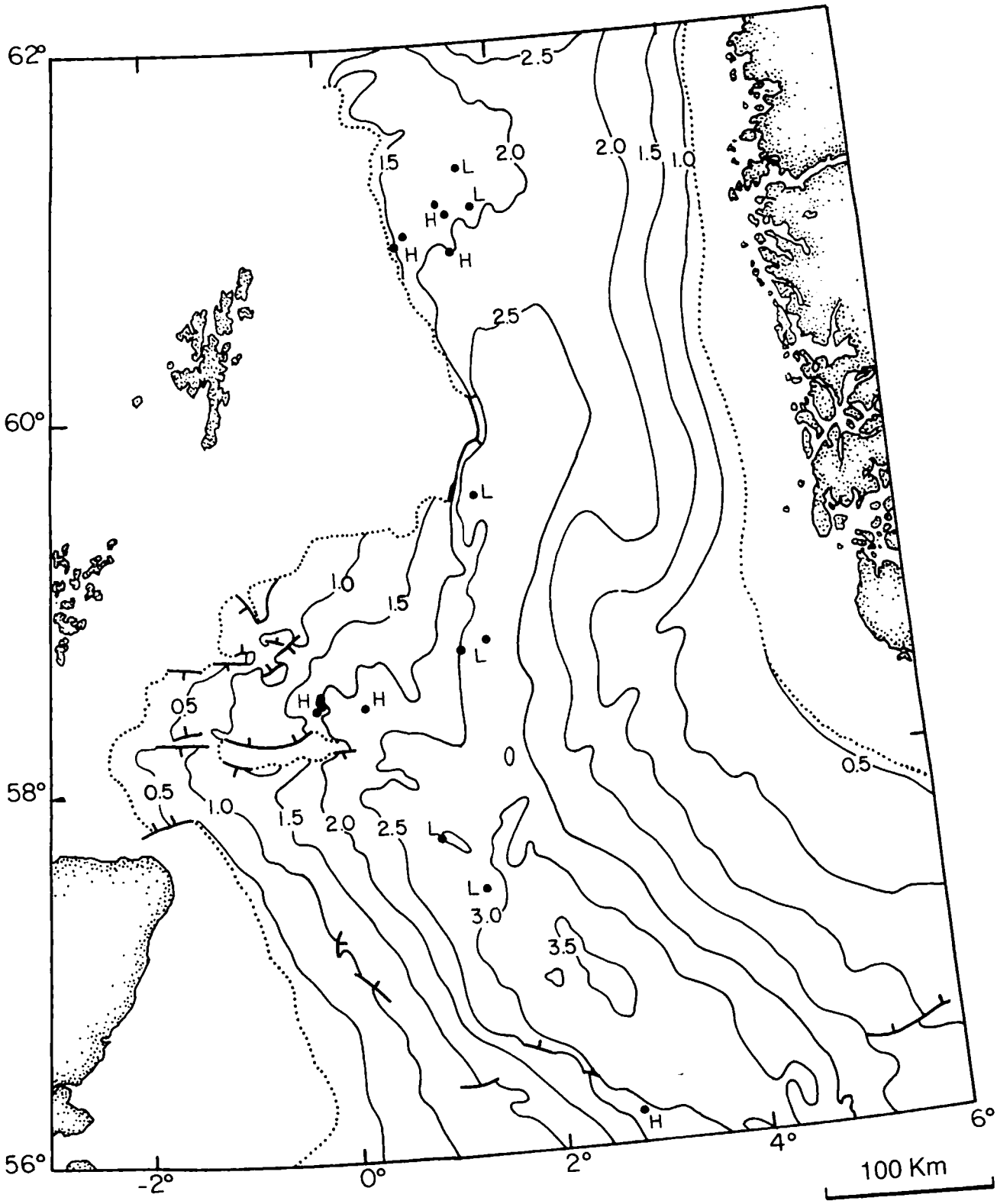


Figure 20—Maturity of organic-rich shales in western North Sea from Mackenzie and McKenzie (1983) are plotted with an H for higher than predicted aromatization (a measure of maturity) or an L for lower than predicted aromatization. Predicted aromatization is based on present-day temperature and two kinetic reaction rate constants for aromatization. However, areas only recently elevated in temperature (rejuvenated) should have lower degree of maturation relative to their present-day temperature than predicted. Locus of Quaternary thermal rejuvenation (Figures 6, 16, and 17) east of points plotted, therefore, may explain why L points occur consistently east of H points. Contour interval = 0.5 km. Dotted line marks boundary of region where Tertiary section is believed complete.

## Appendix 1: Overpressure

Compaction can be viewed most simply as the contraction of a spring (the rock matrix) due to an applied load (the weight of the rock per unit area). In a saturated medium, part of the load is supported by the rock matrix, $L_r$, part by buoyancy, $L_b$, and part by any excess pore pressure in the system, $L_p$. The effective pressure $p_e$ causing mechanical compaction is the net effect of these loads: $p_e = L_r - L_b - L_p$. Void ratio e (volume of water/volume of solids) and porosity $\phi$ (percent water by volume) are experimentally (e.g., Rieke and Chilingarian, 1974) and theoretically (Biot, 1941; Lade, 1980) related by

$$e = \phi/(1 - \phi) = e_o - c_2[\log_{10}(p_e)],$$
$$1 < p_e < 10^{(e_o/c_2)}, \tag{1A}$$

where $e_o$ and $c_2$ are compaction coefficients.

Average overpressure gradient $\lambda$ is equal to the ratio $L_p/(L_r - L_p)$. When $\lambda$ is close to 0, excess pore pressure is also close to 0, and rocks normally consolidate. When sediments are buried with $\lambda$ close to 1, $p_e$ approaches 1 and $\log_{10}(p_e)$ approaches 0 and, thus, from equation 1A, no change of porosity will occur with depth.

The magnitude of $\lambda$ is critical in determining interval tectonic subsidence from equation 1 (see main text). To illustrate this concept, consider the tectonic subsidence represented by interval A: a 1-m thickness of slate (0% porosity) originally deposited as mud with an initial void ratio, $e_o$ of 3 (initial porosity, $\phi_o$, of 0.75). To simplify matters, assume that sediments stratigraphically below interval A consist of sediments of the same lithology as interval A and have a total thickness of S. Setting the change in water depth and sea level to 0, and $\rho_m$, $\rho_g$, $\rho_w$, to 3.33, 2.65, and 1.03 g/cm$^3$, respectively, the tectonic subsidence during interval A from equation 1 is

$$\Delta Y_A = 0.3\Delta R_A + \Delta W_A. \tag{2A}$$

The solid rock isopach, $\Delta R_A$, is determined from the thickness of interval A normalized to 0% porosity which, in this case, is also the present thickness of 1 m. The difference in net thickness of water in the sediment column, $\Delta W_A$, depends, however, on $\lambda$ and S, the total thickness of sediments below interval A. The total thickness of water below interval A before deposition is $W_1 = \phi_{av}S^*$ where $\phi_{av}$ is the average porosity and $S^*$ is the depth to basement at the time of deposition of interval A. When $\lambda = 1$, the pore water $W_1$ remains in the basin and, thus, the total thickness of water after deposition of interval A is $W_2 = \phi_{av}S^* + e_o\Delta R_A$, where $e_o\Delta R_A$ is the added water contained in interval A. If $\lambda = 0$, however, the porosity depth curve, down to depth $S^*$ must be the same before and after deposition of interval A. The total water in the sediment column is the sum of the water above depth $S^*$ and the water present in sediments buried below depth $S^*$ with the deposition of interval A. If $\lambda = 0$, $W_2$ is thus given by

$$W_2 = \phi_{av}S^* + \Delta R_A\{e_o - c_2[\log_{10}(\rho_g gS)]\}, \tag{3A}$$

where we have used equation 1A to determine the void ratio at depth $S^*$. The tectonic subsidence as a function of S and $\lambda$ from equation 2A, therefore, is

$$\Delta Y_A = 0.3 + e_o - (1 - \lambda)c_2[\log_{10}(\rho_g gS)]. \tag{4A}$$

We next develop the theory for determining pore pressure in a sedimentary column. Using Terzaghi and Peck's (1948) theory of one-dimensional consolidation the basic equation of diffusion of excess pore pressure is

$$\partial/\partial z(\alpha\partial u/\partial z) = \partial u/\partial t, \tag{5A}$$

where u is excess head (pressure divided by fluid-unit weight) and $\alpha$ is a diffusion coefficient in cm$^2$/sec$^{-1}$. Note that the coefficient $\alpha$ must be taken inside the first derivative. Because the medium deforms during consolidation, the spatial derivatives contain a hidden advective component.

The diffusion coefficient $\alpha$ can be evaluated from measurements of permeability, k, in darcys by

$$\alpha = k/\mu(1/E_s + \phi/E_w), \tag{6A}$$

where $E_s$ and $E_w$ are the bulk moduli of solid and water, $\mu$ is the viscosity of water, and $\phi$ is the porosity.

The solution of equation 5A describes a simple exponential decay of any initial pressure conditions. Sedimentation adds a driving force equal to the weight of the sediments not supported by buoyancy. In the absence of any other driving mechanism, e.g., aquathermal pressuring, the full equation is

$$\partial/\partial z(\alpha\partial u/\partial z) = \partial u/\partial t - (\rho_s - \rho_w)dS/dt, \tag{7A}$$

where dS/dt is the rate of change of thickness of the sediment column. Boundary conditions are that of no excess head at the surface and no downward flow at the bottom. This second condition is rigorously true only when an impermeable base, such as salt caprock, floors the basin. Solutions to this problem, except for a few special cases, can be obtained only numerically using a modified Crank-Nicholson method (Von Rosenberg, 1977; Thorne, 1985).

The excess pressure gradient is often low in the first kilometer of burial due to the relatively high porosity and permeability of sediments at these depths. With increasing burial, both porosity and permeability decrease in compacting shales commonly causing the development of excess pore pressures. No theoretical relationship has been established that relates porosity and permeability in shales; however, a strong dependence does exist (Von Engelhardt, 1973; Abbott et al. 1981). We have chosen a linear relationship to express this dependence of the form:

$$\log_{10}(k_v) = A + B\phi(1 + \phi). \tag{8A}$$

Values of constants A and B for each time unit can be found in Table 1.

In Figure 21 we show the results of overpressure simulation using these constants for six representative wells. A close comparison between predicted and observed (integrated mud weight) overpressures supports the model assumptions.

## Appendix 2: Estimating Basement Fault Extension

The accuracy of estimates based on regional seismic lines (Christie and Sclater, 1980; Barton and Wood, 1984) on the amount of fault extension across North Sea graben structures is open to some question (Smythe et al, 1980; Ziegler, 1983). Le Pichon and Sibuet (1981) showed that a good estimate of extension factor $\beta$ is

$$\beta_i = \sin(\alpha_i)/\sin(\alpha_i + \theta_i), \tag{9A}$$

where $\theta_i$ is the present angle of tilting of the $i$th bedding plane, $\alpha_i = 180° - \phi$, and $\phi$ is the dip of the fault plane with respect to the bedding plane. Generally, $\beta$ can vary with each bedding plane. The question, then, is whether the resolution of North Sea seismic data is sufficient to determine angles $\theta$ and $\alpha$.

Consider the case in which many small faults break the bedding plane into many small (<200 m) steeply dipping segments forming a sawtooth bedding plane surface. In this case, the seismic wavefront will not see the individual segments. The seismically determined angle of dip, $\theta_s$ can, therefore, be quite different from the true angle of bedding plane dip $\theta$.

To rule out this possibility in the North Sea we have compared, at a number of wells, the seismically determined angle of dip $\theta_s$ on the base Zechstein reflector from Day et al (1981) with the true angle of dip $\theta$ determined from dipmeter logs of Rotliegendes sandstones. Our initial study shows a good agreement between $\theta_s$ and $\theta$ in the wells studied.

The apparent agreement between the angle of dip of the Rotliegendes determined seismically and from dipmeter logs suggests that faults within the North Sea are mappable with seismic data. The relative uncertainty in estimating extension from equation 8A is probably dominated by errors in estimating angle $\alpha$.

Seismic observation of the angle $\alpha$ is complicated because normal faults in the North Sea are generally listric so that the angle $\alpha$ increases with depth. Listric normal faults present in the southern North Sea sole out at two different depths: within the Zechstein (Heybroek, 1975) and at a deep crustal detachment zone (Gibbs, 1983; see also Beach, 1986).

Those faults that sole out within the Zechstein are not directly responsible for crustal extension and, therefore, are not relevant to the problem at hand. The angle $\alpha_z$ of the later type of listric fault at the base Zechstein level is hard to obtain directly from seismic profiles. Heybroek (1975) estimated extension of supra-Zechstein sediments across the Dutch Central graben by balanced reconstruction of regional seismic profiles (G, H, and I in Figure 1). By making the assumption that the extension of the base Zechstein sediments, however, should be equal to the extension of the supra-Zechstein sediments, Gibbs (1983) reconstructed the geometry of basement faults beneath the Zechstein. The angle $\alpha_z$ is found to vary between 120° and 135°. Equivalently, the dip angle of the basement faults ranges between 45° and 60°. The range of uncertainty shown in Figure 9 corresponds to this range in angle $\alpha_z$.

## Appendix 3: Load-Shape Analysis

A full description of load-shape analysis is given in Thorne (1985). In this section we give only a brief summary of the theoretical concepts involved.

Various estimates of the flexural rigidity, $D_i$, of a sedimentary basin during any time interval, i, generally can be determined from contour maps of sedimentary infill, $w_i$, and/or free-air gravity. In the first case, various characteristics of the shape of the sedimentary infill, $w_i$, and the tectonic load, $q_i$, added between times $t_i$ and $t_{i+1}$, can be used to determine the rigidity during the interval $t_i$ to $t_{i+1}$. By comparing successive depositional units, a time history of rigidity can be found. In the second case, free-air gravity anomalies are proportional to the degree of isostatic compensation of each of the loads $q_i$. When a basin is thermally rejuvenated, all of the loads, $q_i$, isostatically adjust in response to the lowering of flexural rigidity. Thus, during a period of thermal rejuvenation, free-air gravity anomalies directly reflect the rigidity of the basin during rejuvenation.

If we know the load, q, and the rigidity, D, the thin elastic plate theory predicts the infill, w. Conversely, if we know q and w, we can invert for D, or if we know D and w, we can invert for q. In load-shape analysis, w is determined from isopach maps after correcting for compaction. The load, q, or the rigidity, D, cannot directly be determined. However, if we make an additional constraining assumption about the shape of q we can find a best-fitting D. Different assumptions about q distinguish the various methods for estimating rigidity.

Three possible assumptions about the load are (1) the load shape remains relatively constant when comparing one stratigraphic unit to the next, (2) basin-forming loads (except for erosion) apply only a downward (not an upward) deflecting force to the basement surface, and (3) loads should be concentrated at one or a few depocenters (the moment of the load(s) about the depocenter(s) should be minimized).

Approximating the degree of error is difficult when estimating rigidity in this way. If the assumptions about the load are correct for any time period, then the derived rigidity will be correct. If the assumptions fail, the derived rigidity will be incorrect. One case in which the assumptions are incorrect is during thermal rejuvenation. The load, in this case, will probably resemble a combination of all previously applied loads (not just the immediately preceding load) due to reactivation of previous basin depocenters. An additional component of the load will be an upward force due to thermal expansion of heated lithosphere. The resulting combination of loads is not likely to meet any of the three assumptions.

## SELECTED REFERENCES


Abbott, D., W. Menke, M. Hobart, and R. Anderson, 1981, Evidence for excess pore pressures in southwest Indian Ocean sediments: Journal of Geophysical Research, v. 86, p. 813-828.

Ahern, J. L., and S. R. Mrkvicka, 1984, A mechanical and thermal model for the evolution of the Williston basin: Tectonics, v. 3, p. 79-102.

Alvarez, F., 1985, Étude de l'evolutionn thermiques basin sedimentaires formes par extension, consequences thermo-mechanique du rifting: application au graben Viking, Mer-du Nord: PhD thesis, Universite de Pierre et Marie Curie, Paris, France, 230 p.

Andrews-Speed, C. P., E. R. Oxburgh, and B. A. Cooper, 1984, Temperatures and depth-dependent heat flow in western North Sea: AAPG Bulletin, v. 68, p. 1764-1781.

Barnard, P. C., and B. S. Cooper, 1981, Oils and source rocks of the North Sea area, *in* L. V. Illing and G. D. Hobson, eds., Petroleum geology of the continental shelf of north-west Europe: London, Institute of Petroleum, p. 169-175.

——— ——— 1983, A review of geochemical data related to the north-west European gas province, *in* J. Brooks, ed., Petroleum geochemistry and exploration of Europe: London, Blackwell Scientific Publications, p. 19-33.

Barton, P., and R. J. Wood, 1984, Tectonic evolution of the North Sea basin: crustal stretching and subsidence: Geophysical Journal of Royal Astronomical Society, v. 79, p. 987-1022.

Beach, A., 1986, A deep seismic reflection profile across the northern North Sea: Nature, v. 323, p. 53-55.

Beaumont, C., 1978, The evolution of sedimentary basins on a viscoelastic lithosphere: theory and examples: Geophysical Journal of the Royal Astronomical Society, v. 55, p. 471-497.

Berggren, W. A., and F. M. Gradstein, 1981, Agglutinated benthonic foraminiferal assemblages in the Palaeogene of the central North Sea: their biostratigraphic and depositional environmental significance, *in* L. V. Illing and G. D. Hobson, eds., Petroleum geology of the continental shelf of north-west Europe: London, Institute of Petroleum, p. 282-288.

Bessis, F., 1986, Some remarks on the study of subsidence of sedimentary basins, application to the Gulf of Lions margin (western Mediterranean): Marine and Petroleum Geology, v. 3, p. 37-63.

Biot, M. A., 1941, General theory of three-dimensional consolidation: Journal of Applied Physics, v. 12, p. 155-164.

Blair, D. G., 1975, Structural styles in North Sea oil and gas fields, *in* A. W. Woodland, ed., Petroleum and the continental shelf of northwest Europe, v. 1: geology: London, Institute of Petroleum, p. 327-338.

Bodine, J., M. S. Steckler, and A. B. Watts, 1981, Observations of flexure and the rheology of the oceanic lithosphere: Journal of Geophysical Research, v. 86, p. 3695-3707.

Boen, F., S. Eggen, and J. Vollset, 1984, 17 structures and basins of the margin from 62° to 69°N and their development, *in* A. M. Spencer, E. Holter, S. O. Johnsen, A. Mørk, E. Nysaether, P. Songstad, and Å. Spinnangr, eds., Petroleum geology of the north European margin: North European Margin Symposium Proceedings, p. 253-270.

Brooks, J., ed., 1983, Petroleum geochemistry and exploration of Europe: London, Blackwell Scientific Publications, 379 p.

Browitt, C. W. A., and R. Newmark, 1981, Seismic activity on the North Sea to April 1981: Edinburgh Institute of Geological Sciences, Global Seismology Unit Report 150.

Bukovics, C., E. G. Cartier, N. D. Shaw, and P. A. Ziegler, 1983, Structure and development of the mid-Norway continental margin, *in* A. M. Spencer et al, eds., Petroleum geology of the north European margin: North European Margin Symposium Proceedings, p. 407-424.

Carstens, H., and K. G. Finstad, 1981, Geothermal gradients of the northern North Sea basin, 59-62°N, *in* L. V. Illing and G. D. Hobson, eds., Petroleum geology of the continental shelf of north-west Europe: London, Institute of Petroleum, p. 152-161.

Caston, V. N. D., 1977, The Quaternary deposits of the central North Sea, 1 and 2: a new isopachyte map of the Quaternary of the North Sea: Institute of Geological Sciences Report 77/11, 22 p.

Chiarelli, A., and F. Duffaud, 1980, Pressure origin and distribution in Jurassic of Viking basin (United Kingdom-Norway): AAPG Bulletin, v. 64, p. 1245-1266.

Christie, P. A. F., and J. G. Sclater, 1980, An extensional origin for the Buchan and Witchground graben in the North Sea: Nature, v. 283, p. 730-733.

Cochran, J. R., 1983, Effect of finite rifting times on the development of sedimentary basin: Earth and Planetary Science Letters, v. 66, p. 289-302.

Collette, B. J., 1960, The gravity field of the North Sea: Delft, Netherlands, W. D. Meinema, 52 p.

Cornelius, C. D., 1975, Geothermal aspects of hydrocarbon exploration in the North Sea area, *in* A. Whiteman, D. Roberts, and M. A. Sellevoll, eds., Petroleum geology and geology of the North Sea and northeast Atlantic continental margin, Norges Geologiske Undersökelse, v. 316, p. 29-68.

Cornford, C., 1984, Source rocks and hydrocarbons of the North Sea, *in* K. W. Glennie, ed., Introduction to the petroleum geology of the North Sea: London, Blackwell Scientific Publications, p. 171-204.

Day, G. A., B. A. Cooper, C. Anderson, W. F. J. Burgers, H. C. Rø nnevik, and H. Schoneich, 1981, Regional seismic structure maps of the North Sea, *in* L. V. Illing and G. D. Hobson, eds., Petroleum geology of the continental shelf of north-west Europe: London, Institute of Petroleum, p. 76-84.

De'Ath, N. G., and S. F. Schuyleman, 1981, The geology of the Magnus oilfield, *in* L. V. Illing and G. D. Hobson, eds., Petroleum geology of the continental shelf of north-west Europe: London, Institute of Petroleum, p. 342-351.

Dewey, J. F., 1982, Plate tectonics and the evolution of the British Islands: Journal of the Geological Society of London, v. 139, p. 371-412.

Dikkers, A. J., 1977, Sketch of a possible lineament pattern in northwest Europe: Geologie en Mijnbouw, v. 56, p. 275-285.

Dimitropoulos, K., and J. Donato, 1982, Sedimentary basin development in the northern North Sea and Moray Firth (abs.): European Geophysical Society Programme and Abstracts, p. 75.

Donato, J. A., and M. C. Tully, 1981, A regional interpretation of North Sea gravity data, *in* L. V. Illing and G. D. Hobson, eds., Petroleum geology of the continental shelf of north-west Europe: London, Institute of Petroleum, p. 65-75.

——— ——— 1982, A proposed granite batholith along the western flank of the North Sea Viking graben: Geophysical Journal of the Royal Astronomical Society, v. 69, p. 187-195.

Eynon, G., 1981, Basin development and sedimentation in the Middle Jurassic of the northern North Sea, *in* L. V. Illing and G. D. Hobson, eds., Petroleum geology of the continental shelf of north-west Europe: London, Institute of Petroleum, p. 196-204.

Fagerland, N., 1983, Tectonic analysis of a Viking graben border fault: AAPG Bulletin, v. 67, p. 2125-2136.

Falvey, D. A., 1974, The development of continental margins in plate tectonic theory: Australian Petroleum Exploration Association Journal, v. 14, p. 95-106.

Finstad, K. G., 1975, Review of the offshore Jurassic of the UK northern North Sea, *in* K. G. Finstad and R. C. Selly, eds., Northern North Sea Symposium: Norwegian Petroleum Society, v. 2, p. 1-24.

Fisher, M. J., 1984, Triassic of the North Sea, *in* K. W. Glennie, ed., Introduction to the petroleum geology of the North Sea: London, Blackwell Scientific Publications, p. 85-101.

——— and J. A. Miles, 1983, Kerogen types, organic maturation and hydrocarbon occurrences in the Moray Firth and south Viking graben, North Sea basin, *in* J. Brooks, ed., Petroleum geochemistry and exploration of Europe: London, Blackwell Scientific Publications, p. 195-202.

Fowler, C. M. R., and E. G. Nisbet, 1984, The subsidence of the Williston basin: Canadian Journal of Earth Science, v. 22, p. 408-415.

Frost, R. T. C., F. J. Fitch, and J. A. Miller, 1981, The age and nature of the crystalline basement of the North Sea basin, *in* L. V. Illing and G. D. Hobson, eds., Petroleum geology of the continental shelf of north-west Europe: London, Institute of Petroleum, p. 43-57.

Garner, D. L., and D. L. Turcotte, 1984, The thermal and mechanical evolution of the Anadarko basin: Tectonophysics, v. 107, p. 1-24.

Gibbs, A. D., 1983, Balanced cross-section construction from seismic sections in areas of extensional tectonics: Journal of Structural Geology, v. 5, p. 153-160.

Glennie, K. W., 1984, The structural framework and the pre-Permian history of the North Sea area, *in* K. W. Glennie, ed., Introduction to the petroleum geology of the North Sea: London, Blackwell Scientific Publications, p. 17-40.

——— and P. L. E. Boegner, 1981, Sole pit inversion tectonics, *in* L. V. Illing and G. D. Hobson, eds., Petroleum geology of the continental shelf of north-west Europe: London, Institute of Petroleum, p. 110-120.

Goff, J. C., 1983, Hydrocarbon generation and migration from Jurassic source rocks in the E. Shetland basin and Viking graben of the northern North Sea: Journal of the Geological Society of London, v. 140, p. 445-474.

Gowers, M. B., and A. Saeboe, 1985, On the structural evolution of the Central Trough in the Norwegian and Danish sectors of the North Sea: Marine and Petroleum Geology, v. 2, p. 298-326.

Gray, W. D. T., and G. Barnes, 1981, The Heather oil field, *in* L. V. Illing and G. D. Hobson, eds., Petroleum geology of the continental shelf of north-west Europe: London, Institute of Petroleum, p. 335-341.

Guidish, T. M., C. Kendall, I. Lerche, D. J. Toth, and R. F. Yarzab, 1985, Basin evaluation using burial history calculations: an overview: AAPG Bulletin, v. 69, p. 92-105.

Hallet, D., 1981, Refinement of the geological model of the Thistle field, *in* L. V. Illing and G. D. Hobson, eds., Petroleum geology of the continental shelf of north-west Europe: London, Institute of Petroleum, p. 315-325.

Halstead, P. H., 1975, Northern North Sea faulting, *in* K. G. Finstad and R. C. Selley, eds., Jurassic northern North Sea Symposium: Norwegian Petroleum Society, p. 10/1-38.

Hamar, G. P., T. Fjaeran, and A. Hesjedal, 1983, Jurassic stratigraphy of the south-southeastern Norwegian offshore: Geologie en Mijnbouw, v. 62, p. 103-114.

Haq, B. U., J. Hardenbol, and P. R. Vail, 1987, Chronology of fluctuating sea levels since the Triassic (250 million years ago to present): Science, v. 235, p. 1156-1166.

Harding, T. P., 1983, Graben hydrocarbon plays and structural styles: Geologie en Mijnbouw, v. 62, p. 3-24.

Haxby, W. F., D. L. Turcotte, and J. M. Bird, 1976, Thermal and mechanical evolution of the Michigan basin: Tectonophysics, v. 36, p. 57-75.

Hay, J. T. C., 1978, Structural development in the northern North Sea: Journal of Petroleum Geology, v. 1, p. 65-77.

Heybroek, P., 1974, Explanation to tectonic maps of the Netherlands: Geologie en Mijnbouw, v. 53, p. 43-50.

——— 1975, On the structure of the Dutch part of the central North Sea Graben, *in* A. W. Woodland, ed., Petroleum and the continental shelf of north-west Europe, volume 1: geology: London, Institute of Petroleum Applied Science Publication, p. 339-352.

Hobbs, P., and D. Long, 1977, Geotechnical testing of North Sea sediments from "Ferder" borehole 77/79: Institute of Geological Sciences Report 78/15.

Illing, L. V., and G. D. Hobson, eds., Petroleum geology of the continental shelf of north-west Europe: London, Institute of Petroleum, 521 p.

Jarvis, G. T., and D. P. McKenzie, 1980, Sedimentary basin formation with finite extension rates: Earth and Planetary Science Letters, v. 48, p. 42-52.

Johnson, R. J., and R. G. Dingwall, 1981, The Caledonides: their influence on the stratigraphy of the northwest European continental shelf, *in* L. V. Illing and G. D. Hobson, eds., Petroleum geology of the continental shelf of north-west Europe: London, Institute of Petroleum, p. 85-97.

Jowett, E. C., and G. T. Jarvis, 1984, Formation of foreland rifts: Sedimentary Geology, v. 40, p. 51-72.

Karlson, W., 1978, Tertiary clay in the North Sea, *in* M. M. Mortland and V. C. Farmer, eds.: International Clay Conference, p. 284-290.

Karner, G. D., 1982, Spectral representations of isostatic models: BMR Journal of Australian Geology and Geophysics, v. 7, p. 55-62.

——— M. S. Steckler, and J. A. Thorne, 1983, Long-term thermomechanical properties of the continental lithosphere: Nature, v. 304, p. 250-253.

Kent, P. E., 1976, Major synchronous events in continental shelves: Tectonophysics, v. 36, p. 87-91.

Kusznir, N., and G. Karner, 1985, Dependence of the flexural rigidity of the continental lithosphere on rheology and temperature: Nature, v. 316, p. 138-142.

Lade, P. V., 1980, Stress-strain theory for normally consolidated clay, *in* Numerical methods in geomechanics: 3rd International Conference on Numerical Methods in Geomechanics Proceedings, v. 4, p. 1325-1340.

Le Pichon, X., and J. C. Sibuet, 1981, Passive margins: a model of formation: Journal of Geological Research, v. 86, p. 3708-3720.

Mackenzie, A. S., and D. P. McKenzie, 1983, Isomerisation and aromatisation of hydrocarbons in sedimentary basins formed by extension: Geological Magazine, v. 120, p. 417-470.

Magara, K., 1978, Compaction and fluid migration: practical petroleum geology: developments in petroleum science, 9: Amsterdam, Elsevier, 320 p.

Maher, C. E., 1981, The Piper oilfield, *in* L. V. Illing and G. D. Hobson, eds., Petroleum geology of the continental shelf of north-west Europe: London, Institute of Petroleum, p. 358-370.

McKenzie, D., 1984, A possible mechanism for epeirogenic uplift: Nature, v. 307, p. 616-618.

McKenzie, D. P., 1978, Some remarks on the development of sedimentary basins: Earth and Planetary Science Letters, v. 40, p. 25-32.

——— and C. Bowin, 1976, The relationship between bathymetry and gravity in the Atlantic Ocean: Journal of Geophysical Research, v. 81, p. 1903-15.

Michelson, O., and C. Anderson, 1983, Mesozoic structural and sedimentary development of the Danish Central graben: Geologie en Mijnbouw, v. 62, p. 93-102.

Middleton, M. F., 1980, A model of intracratonic basin formation, entailing deep crustal metamorphism: Geophysical Journal of the

Royal Astronomical Society, v. 62, p. 1-14.
Norwegian Petroleum Directorate, 1976, Lithology well reports: Norwegian Petroleum Directorate Papers #1-20.
Nunn, J. A., 1981, Thermal contraction and flexure of intracratonic basins: PhD thesis, Northwestern University, Evanston, Illinois, 353 p.
——— N. H. Sleep, and W. E. Moore, 1984, Thermal subsidence and generation of hydrocarbons in Michigan basin: AAPG Bulletin, v. 68, p. 296-315.
Pannekoek, A. J., 1954, Tertiary of the Netherlands: Geologie en Mijnbouw, v. 16e, p. 156-162.
Pegrum, P. M., G. Rees, and D. Naylor, 1975, Geology of the northwest European continental shelf, v. 2: the North Sea: London, Graham, Trotman and Dudley, 224 p.
Poskitt, T. J., 1969, Consolidation of a saturated clay with variable permeability and porosity: Geotechnique, v. 19, p. 234-252.
Rieke, H. H., and G. V. Chilingarian, 1974, Compaction of argillaceous sediments: Amsterdam, Elsevier, 424 p.
Rønnevik, H., S. Eggen, and J. Vollset, 1983, Exploration of the Norwegian Shelf, *in* J. Brooks, ed., Petroleum geochemistry and exploration of Europe: London, Blackwell Scientific Publications, p. 71-94.
Royden, L., and C. E. Keen, 1980, Rifting processes and thermal evolution of the continental shelf of eastern Canada determined from subsidence curves: Earth and Planetary Science Letters, v. 51, p. 343-361.
——— J. G. Sclater, and R. P. Von Herzen, 1980, Continental margin subsidence and heat flow: important parameters in formation of petroleum hydrocarbons: AAPG Bulletin, v. 64, p. 173-187.
Scholle, P. A., 1977, Deposition, diagenesis, and hydrocarbon potential of "deeper-water" limestones: AAPG Continuing Education Course Note Series 7, 25 p.
Sclater, J. G., and P. A. F. Christie, 1980, Continental stretching: an explanation of the post-mid-Cretaceous subsidence of the central North Sea basin: Journal of Geophysical Research, v. 85, p. 3711-3739.
Skempton, A. W., 1970, The consolidation of clays by gravitational compaction: Geological Society of London Quarterly Journal, v. 125, p. 373-411.
Skjerven, J., F. Rijs, and J. E. Kalheim, 1983, Late Paleozoic to early Cenozoic structural development of the south-southeastern Norwegian North Sea: Geologie en Mijnbouw, v. 62, p. 35-46.
Smythe, D. K., A. G. Skuce, and J. A. Donato, 1980, Geological objections to an extensional origin for the Buchan and Witchground graben in the North Sea: Nature, v. 287, p. 467-468.
Solli, M., 1976, En Seismisk Skorpeunderøkelse Norges Shetland: PhD thesis, University of Bergen, Bergen, Norway.
Steckler, M., 1981, The thermo-chemical evolution of Atlantic-type continental margins: PhD thesis, Columbia University, New York, New York, 251 p.
——— and A. B. Watts, 1978, Subsidence of the Atlantic-type continental margin off New York: Earth and Planetary Science Letters, v. 41, p. 1-13.
Surlyk, F., 1978, Jurassic basin evolution of east Greenland: Nature, v. 274, p. 130-133.
Strang van Hess, G. L., 1981, Gravity measurements on the North Sea (abs.): EOS, v. 62, p. 815.
Terzaghi, K., and R. B. Peck, 1948, Soil mechanics in engineering practice: New York, Wiley, 566 p.
Thorne, J. A., 1985, Studies in stratology: the physics of stratigraphy: PhD thesis, Columbia University, New York, New York, 523 p.
Threlfall, W. F., 1981, Structural framework of the central and northern North Sea, *in* L. V. Illing and G. D. Hobson, eds., Petroleum geology of the continental shelf of north-west Europe: London, Institute of Petroleum, p. 98-103.
Vail, P. R., and R. G. Todd, 1981, Northern North Sea Jurassic unconformities, chronostratigraphy and sea-level changes from seismic stratigraphy, *in* L. V. Illing and G. D. Hobson, eds., Petroleum geology of the continental shelf of north-west Europe: London, Institute of Petroleum, p. 216-235.
Van Hinte, J. E., 1978, Geohistory analysis—application of micropaleontology in exploration geology: AAPG Bulletin, v. 62, p. 201-222.
Von Engelhardt, W., 1973, Die bildung von sedimenten und sedimentgesteinen: Stuttgart, Schweizerbart'sche Verlagsbuchhandlung, 378 p.
Von Rosenberg, D. U., 1977, Methods for the numerical solution of partial differential equations: Tulsa, Farrar & Associates, 128 p.
Waples, D. W., 1980, Time and temperature in petroleum formation: application of Lopatin's method to petroleum exploration: AAPG Bulletin, v. 64, p. 916-926.
Warpinski, N. E., 1986, Elastic and viscoelastic model of the stress history of sedimentary rocks: Sandia National Lab Open File Report 86-0238, 85 p.
Watts, A. B., 1978, An analysis of isostasy in the world's oceans, 1, Hawaiian-Emperor Seamount Chain: Journal of Geophysical Research, v. 83, p. 5989-6004.
——— and M. S. Steckler, 1979, Subsidence and eustacy at the continental margin of eastern North America, *in* M. Talwani, S. Hay, and W. Ryan, eds., Deep drilling results in the Atlantic Ocean: continental margins and paleoenvironment, Maurice Ewing Series 3: American Geophysical Union, p. 218-234.
——— and J. A. Thorne, 1984, Tectonics, global changes in sea-level and their relationship to stratigraphic sequences at the U.S. Atlantic continental margin: Marine and Petroleum Geology, v. 1, p. 319-339.
——— G. D. Karner, and M. S. Steckler, 1982, Lithospheric flexure and the evolution of sedimentary basins: Philosophical Transactions of the Royal Society of London A:305, p. 249-281.
Welte, D. H., M. A. Yukler, M. Radke, D. Leythaeuser, U. Mann, and U. Ritter, 1983, Organic geochemistry and basin modeling—important tools in petroleum exploration, *in* J. Brooks, ed., Petroleum geochemistry and exploration of Europe: London, Blackwell Scientific Publications, p. 237-252.
Wickham, S. M., and E. R. Oxburgh, 1985, Continental rifts as a setting for regional metamorphism: Nature, v. 318, p. 330-333.
Wood, R., and P. Barton, 1983, Crustal thinning and subsidence in the North Sea: Nature, v. 302, p. 134-136.
Wood, R. J., 1982, Subsidence in the North Sea: PhD thesis, Cambridge University, Cambridge, England, 94 p.
Woodland, A. W., ed., 1975, Petroleum and the continental shelf of north-west Europe: v. 1: geology: London, Institute of Petroleum, 501 p.
Zielger, P. A., 1978, North-western Europe: tectonics and basin development: Geologie en Minjbouw, v. 57, p. 589-626.
——— 1981, Evolution of sedimentary basins in north-west Europe, *in* L. V. Illing and G. D. Hobson, eds., Petroleum geology of the continental shelf of north-west Europe: London, Institute of Petroleum Applied Science Publication, p. 3-39.
——— 1982, Geological atlas of western and central Europe: Amsterdam, Elsevier, 131 p.
——— 1983, Crustal thinning and subsidence in the North Sea: Nature, v. 304, p. 561.
——— 1984, Caledonian and Hercynian crustal consolidation of western and central Europe—a working hypothesis: Geologie en Mijnbouw, v. 63, p. 93-108.
——— and C. J. Louwerens, 1979, Tectonics of the North Sea, *in* E. Oele, R. T. E. Schuttenhelm, and A. J. Wiggers, eds., The Quaternary history of the North Sea: Acta Univérsity Uppsala Symposium Uppsala Annum Quingentesimum Celebrantis: 2. Uppsala, p. 7-22.
Ziegler, W. H., 1975, Outline of the geological history of the North Sea, *in* A. W. Woodland, ed., Petroleum and the continental shelf of north-west Europe, volume 1: geology: London, Institute of Petroleum, p. 165-190.